Check for updates

ADVANCED THERAPEUTICS
www.advtherap.com

Cocktail Polyplexes With Synchronous Flightless I siRNA and Nitric Oxide Release for Potential Chronic Wound Healing

Mahshid Kharaziha, Sahar Salehi,* and Thomas Scheibel*

Chronic wounds are one of the health challenges threatening human life. In these wounds, overexpression of some types of cytoskeletal actin-remodeling proteins including Flightless I (Flii) can often lead to severe skin scarring. Herein, arginine functionalized poly(β-amino ester)s are synthesized to develop polyplexes with alginate for delivery of Flii siRNA. This approach results in forming polyplexes with distinct features, such as tunable zeta potential, particle size, polydispersity, and arginine conjugation level. It is demonstrated that the uptake of arginine functionalized poly(β-amino ester)/alginate particles is composition-dependent for various cell types including J774.1 macrophages and BJ fibroblasts. Such polyplexes trigger nitric oxide release by macrophages enhancing the expression of anti-inflammatory genes while diminishing the expression of pro-inflammatory markers and demonstrating its immunomodulatory properties. Flii siRNA loaded particles provide condensed siRNA into the core-shell polyplex and exhibit controlled release of Flii siRNA over 24 h. The uptake rate of this polyplex by macrophages and fibroblasts is higher than that of a commercial gene carrier (Lipofectamine 2000), knocking down the in vitro Flii gene expression (1.3-fold). The increased BJ fibroblast proliferation and higher expression of collagen I (COL I) show the suitability of these polyplexes for wound healing.

1. Introduction

Wound healing is a dynamic and well-organized biological process that remodels soft tissues after damage. Any disruption in cellular and molecular processes frequently results in wound healing failure and chronic wounds.[1] The inflammatory reactions, especially, are critical in the early stages of wound healing as macrophages are involved in the healing process.[2] Macrophages are adaptable cells that undergo phenotypic changes throughout the wound-healing cascade. The M1 phenotype promotes inflammation, whereas the M2 phenotype supports anti-inflammatory responses and facilitates healing.[3] Chronic wounds (i.e., autoimmune diseases) are distinguished by elevated levels of M1 and intensified pro-inflammatory responses.[4,5] The main result of chronic wounds is the abnormal expression of proteins participating in the dynamic remodeling and regulation of the actin cytoskeleton, e.g., Flightless I (Flii).[6] Consequently, patients with these chronic wounds experience chronic inflammation and scarring on both the skin and mucous membranes.[7] In this scenario, the restoration of collagen expression

M. Kharaziha
Department of Materials Engineering
Isfahan University of Technology
84156-83111 Isfahan, Iran
E-mail: kharaziha@iut.ac.ir

M. Kharaziha, S. Salehi, T. Scheibel
Department of Biomaterials, Faculty of Engineering Science
University of Bayreuth
95447 Bayreuth, Germany
E-mail: Sahar.Salehi@uni-bayreuth.de

T. Scheibel
Bayreuther Zentrum für Kolloide und Grenzflächen (BZKG)
University of Bayreuth
95447 Bayreuth, Germany

T. Scheibel
Bayreuther Zentrum für Molekulare Biowissenschaften (BZMB)
University of Bayreuth
95447 Bayreuth, Germany

T. Scheibel
Bayreuther Materialzentrum (BayMAT)
University of Bayreuth
95447 Bayreuth, Germany

T. Scheibel
Bayerisches Polymerinstitut (BPI)
University of Bayreuth
95447 Bayreuth, Germany

The ORCID identification number(s) for the author(s) of this article can be found under https://doi.org/10.1002/adtp.202400329

© 2024 The Author(s). Advanced Therapeutics published by Wiley-VCH GmbH. This is an open access article under the terms of the Creative Commons Attribution License, which permits use, distribution and reproduction in any medium, provided the original work is properly cited.

DOI: 10.1002/adtp.202400329

through gene therapy is considered one of the most promising strategies.[8] Furthermore, due to the chronic nature of these wounds, any approach that can speed up the transition from the M1 to M2 stage is desirable. This transition can shift the wound status from the inflammatory phase to the proliferation stage in the wound healing cascade.[9] Therefore, the main focus of this study is the combination of these two strategies defined as increasing the collagen type VII level and M1-to-M2 phenotype transition of macrophages.

The application of the gene therapy approach for the treatment of chronic wounds has been focused on the expression level of collagen type VII using gene-modified autologous fibroblasts[10] as well as delivery of 2′-O-methyl antisense oligoribonucleotides (AONs).[11] In this study, we proposed gene silencing using small interfering RNA (siRNA) to control M1 phenotype pathways of macrophages and to improve the wound healing process by blocking the Flii gene expression. Previous studies have shown that silencing Flii gene expression using Flii siRNA in cultured keratinocytes resulted in improved cell proliferation, migration, and wound healing rate.[12] However, the poor efficiency of siRNA delivery across the cell's membrane and its rapid degradation due to endogenous nuclease action has made siRNA therapeutics challenging.[13] As an alternative, nanocarriers loaded with siRNA can protect them from degradation while accelerating the intracellular delivery.[14] Different carriers have been investigated as vectors to protect siRNA, including viruses, lipid nanoparticles (NPs), metal, metal oxide NPs, and polymers.[15] These complexes have been designed to preserve siRNA integrity, increase cellular uptake, provide efficient siRNA delivery, and simplify its entry to the cell membrane. Since siRNA delivery does not need admittance to the nucleus, synthetic vectors are preferred to virus carriers owing to their biological safety and cost-effectiveness.[16] Furthermore, cationic polymers are preferred over liposomes and metal oxides due to their low toxicity and improved endosomal escape compared to liposomes, lipid formulations, and metal oxides.[17] Cationic polymers form ionic complexes with the anionic phosphate backbone of siRNA and protect endosomal escape after endocytic uptake.[18] The common cationic polymers applied for siRNA delivery are chitosan[19] and polyethyleneimine.[20] Poly(β-amino ester)s (PAE), a more recent cationic polymer, is used for delivering nucleic acid and they provide high efficiency of transfection, as well as high biocompatibility and specificity within in vitro gene delivery.[8,21] Unlike lipid-based NPs, which carry RNA therapeutics in a liposome structure, PAE particles hold RNA within their matrix and tolerate higher encapsulation and RNA interference (RNAi) loading efficiencies. PAEs, via electrostatic interactions, can neutralize negatively charged siRNA to create discrete particles, called polyplexes.[22] The positively charged polyplexes adhere to cell membranes and are transported into the cytoplasm through endosomal transport. However, the weak colloidal stability of these complexes often led to the burst release of siRNA, thus, restricting their applications.[23] Moreover, owing to highly positively charged surfaces, these cationic polymers could not only interact with cell surfaces but also with other charged surfaces, leading to decreased delivery efficiency.[24] To overcome these issues, various complex approaches have been recommended to tailor the surface charge and compositions via surface coatings using hydrophilic polymers, copolymerization, and polymer conjugation.[25,26] For instance, the modulation of surface charge and hydrophobicity of PAEs have been addressed via end-capping or functionalization strategies. A vast library of oligopeptide moieties based on arginine (Arg) can compact larger quantities of RNA enhancing the polyplex density, leading to improved stability, transfection efficiency, and better biological performance.[27,28] In this structure, the release of nitric oxide (NO) resulting from Arg metabolism can directly regulate the inflammation, proliferation, and angiogenesis phases.[29,30] Moreover, Arg residues on the surface of particles could inspire the virus vectors providing exceptional transmembrane function and biosafety of cell-penetrating peptides (CPPs).[31,32] Therefore, this strategy is desired to expedite wound healing, particularly in chronic wounds, while enhancing siRNA transfection simultaneously. Another favorable strategy to improve in vivo gene stability is the creation of ternary complexes by protecting the cationic charges of branched PAEs with an anionic polymer layer, based on poly(L-glutamic acid).[26,33] This anionic polymer on the polyplexes could create a negatively charged shell, decreasing the non-specific binding of cationic charge polyplexes to physiological molecules.[34] According to the natural anionic properties of alginate, it could be one biomaterial to promote the transfection efficiency of siRNA in vitro, while preserving its biocompatibility and low toxicity to cells. To our knowledge, the formation of Arg-grafted PAE (Arg-N-PAE)/alginate (APA) particles for siRNA delivery has not been investigated yet.

In the present work, self-assembled polyplex particles were utilized to directly deliver Flii siRNA in vitro and to induce macrophage reprogramming from the pro-inflammatory (M1) to the anti-inflammatory (M2) phenotype as well as to promote collagen deposition by BJ fibroblasts. The cocktail polyplex consists of 2 cationic components, Arg and PAE, which are conjugated, plus anionic alginate which creates a negatively charged shell. These 3 components were mixed in specific ratios to form stable NPs that could efficiently deliver Flii siRNA to target cells. In this strategy, the synergic role of Flii siRNA delivery and Arg metabolism was considered and modulated using Arg-PAE conjugates with various ratios and alginate complexation. An in vitro scratch assay was conducted to assess the effectiveness of the cocktail polyplex in promoting wound healing. The potential of this newly designed particle for treating autoimmune disease was explored by enhancing gene silencing and accelerating an in vitro wound healing cascade.

2. Results and Discussion

2.1. Physiochemical Characterization of APA Particles

To create APA particles, the PAE backbone was first synthesized via the conjugation of N, N-dimethylethylenediamine, and 1,4-butanediol diacrylate in a one-step Michael addition reaction. The proton nuclear magnetic resonance (^{1}H-NMR) spectrum (shown in Figure S1, Supporting Information) confirmed the formation of the expected structure of PAE shown in **Figure 1A**. The ^{1}H-NMR spectrum of PAE consisted of the identified peaks of the backbone protons in the region of $\delta = 3$–4 ppm. The ester groups in the PAE backbone typically gave rise to peaks in the region of $\delta = 4.0$–4.5 ppm, while the amino groups in the side chains

© 2024 The Author(s). Advanced Therapeutics published by Wiley-VCH GmbH

23663987, 2024, 12, Downloaded from https://advanced.onlinelibrary.wiley.com/doi/10.1002/adtp.202400329 by Universitaet Bayreuth, Wiley Online Library on [14/03/2025]. See the Terms and Conditions (https://onlinelibrary.wiley.com/terms-and-conditions) on Wiley Online Library for rules of use; OA articles are governed by the applicable Creative Commons License

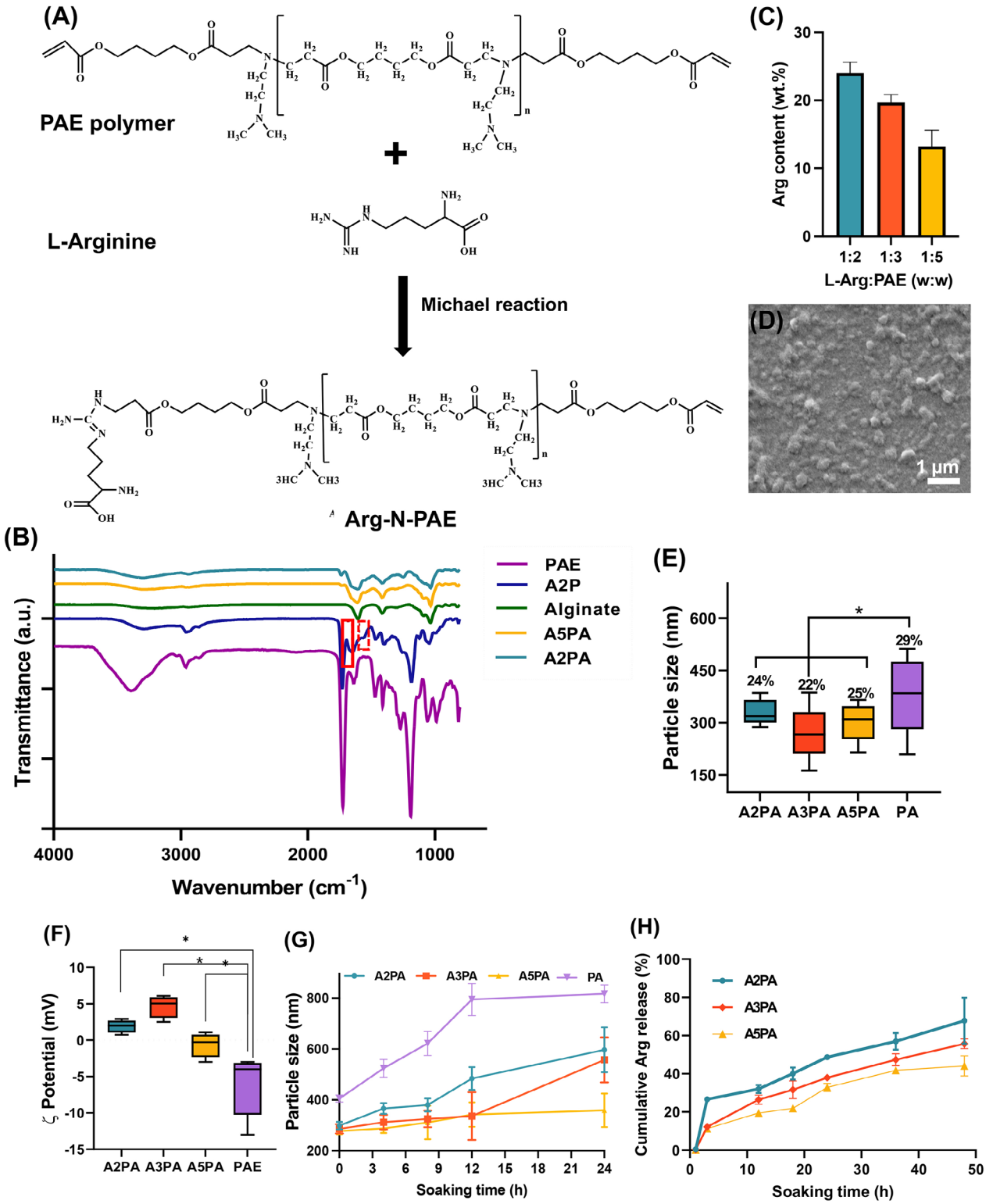

Figure 1. Physiochemical characterization of Arg-N-PAE (AP)/alginate (APA) particles: A) Illustration showing the structure and synthesis process of Poly(β-amino ester) (PAE) and Arg-N-PAE (AP) copolymers, B) FTIR spectra of PAE, alginate and A2P polymers as well as A2P/alginate (A2PA) and A5P/alginate (A5PA) particles, C) The Arg content conjugated to PAE polymer in various AP copolymers, D) Scanning electron microscopy (SEM) image of A3P/alginate (A3PA) particles, E) The average hydrodynamic diameter (PDI was calculated for each particle types and presented on each block), F) the Zeta potentials of APA and arginine-free PAE/alginate (PA) particles. Findings are present as the mean (n = 3) ± SD (*: statistical difference, $P < 0.05$), G) The average hydrodynamic diameter of APA and PA particles, with prolonged soaking in PBS solution for 24 h, H) The Arg release from APA particles over 48 h incubation in PBS solution.

© 2024 The Author(s). Advanced Therapeutics published by Wiley-VCH GmbH

23663987, 2024, 12, Downloaded from https://advanced.onlinelibrary.wiley.com/doi/10.1002/adtp.202400329 by Universitaet Bayreuth, Wiley Online Library on [14/03/2025]. See the Terms and Conditions (https://onlinelibrary.wiley.com/terms-and-conditions) on Wiley Online Library for rules of use; OA articles are governed by the applicable Creative Commons License

of the polymer could give rise to peaks in the region of δ = 2.5 ppm. Next, the end-acrylate groups were further modified using arginine (Arg-N-PAE) with various Arg: PAE weight ratios (1:2 (A2P), 1:3 (A3P), and 1:5 (A5P)). The proton nuclear magnetic resonance (^{1}H-NMR) spectrum of A2P copolymer is provided as an example of Arg-N-PAE copolymer in Figure S2 (Supporting Information). Arg conjugation was verified by detecting two distinct peaks attributed to methylene groups in Arg at δ = 1.53 and 3.00 ppm. In addition, the conjugation degree of Arg in A2P was calculated at 12.8% using the peak area (the ratio of the peak at 1.53 ppm to the peak at 2.5 ppm) in the ^{1}H-NMR spectrum. This value was near to other Arg-conjugated polymers.[29] It should be noted that the acrylate signal was only identified in the PAE spectrum, and it vanished after the Arg reaction, confirming the conjugation of the Arg group. The ^{1}H-NMR spectrum of the A2P copolymer agrees with previously published data for the Arg-modified polymers.[28,35] In Figure 1B, the Fourier Transform Infrared (FTIR) spectrum of the A2P (an example of Arg-N-PAE copolymer), is shown and compared with the PAE spectrum. The C—O bond visible at 1181 cm^{-1}, C═O stretching at 1700–1750 cm^{-1}, aliphatic C—H stretching vibration in the region of 2850–3000 cm^{-1}, N—H stretching vibration at 1650–1700 cm^{-1}, and N—H stretching vibration in the region of 3200–3500 cm^{-1} confirmed PAE polymer.[36] In addition, an amide I band in the spectrum of A2P can be identified in the region of 1600–1700 cm^{-1}, arising from the carbonyl (C═O) stretching vibrations in the Arg chain. An amide II band was identified at 1500–1600 cm^{-1}, and the presence of the C—N bond of the Arg side chain at 1000–1100 cm^{-1} confirmed the conjugation of Arg to the PAE network.[29] These peaks were highlighted with red rectangles. Both ^{1}H-NMR and FTIR spectra confirmed the formation of Arg-N-PAE copolymers. Our results indicate that Arg can react with the PAE backbone through a Michael reaction by double-binding PAE as an electrophile and the amine group of Arg as a nucleophile. This process is illustrated in Figure 1A. However, to enhance the bioactivity and degradation rate of Arg-N-PAE copolymer, 1-(3-Dimethylaminopropyl)-3-ethyl carbodiimide hydrochloride/ N-hydroxysuccinimide (EDC/NHS) was used in the synthesis process. When EDC/NHS is present in the reaction, it is expected that Arg will couple to PAE via a classic amidation reaction, as illustrated in Figure S3 (Supporting Information). EDC/NHS could facilitate nucleophilic attack and stabilize the transition states. EDC reacts with carboxyl groups of esters on the PAE polymer. In this reaction, the activated PAE further reacts with the NHS to form an NHS ester intermediate. The Arg molecule also reacts with the NHS ester intermediate to form a stable amide bond between the carboxyl group on the PAE polymer and the amine group on the Arg molecule. The presence of amide groups was also confirmed by the FTIR spectrum of A2P. Our results revealed that owing to the small amount of EDC/NHS, this reaction not only did not degrade the polymer network but also may have an effective role in bioactivity and biodegradation rate. The Arg content of each copolymer was determined using the Sakaguchi method. Figure 1C shows with decreasing Arg: PAE weight ratio from 1:2 (A2P) to 1:5 (A5P), the Arg content decreased from 24 ± 1 wt.% to 13 ± 2 wt.%. The efficiency of this conjugation process increased from 72 to 78 wt.% when the Arg: PAE ratio was raised to 1:3. However, when the Arg: PAE ratio was elevated to 1:2, the conjugation efficiency decreased to ≈72 wt.%. This reduction may be due to the increased steric hindrance caused by the Arg side chain. Moreover, the higher charge density in the reaction mixture could also be a factor preventing high Arg conjugation. Therefore, the Arg content in the copolymers was chosen to be within the optimized range of 13–24 wt.% (correlated with an Arg: PAE weight ratio of 1:2-1:5).

Following the Arg-N-PAE (AP) copolymer synthesis, Arg-N-PAE/alginate (APA) particles were formed using a polyelectrolyte complexation process. Scanning electron microscopy (SEM) image in Figure 1D confirmed spherical particle formation with a diameter of less than 500 nm. To study the formation of particles in various Arg-N-PAE: alginate weight ratios (2:1, 1:1, and 1:2) the dynamic light scattering (DLS) analysis was performed. Figure 1E and Table S2 (Supporting Information) show the dynamic size of particles in various samples. Previous studies have shown that particles suitable for cellular uptake should be less than 300 nm in size. Additionally, particles with less negative surface charges have better interactions with cell surfaces.[37] Therefore, we determined the best Arg-N-PAE: alginate weight ratio in A2PA (1:1), A3PA (1:1), and A5PA (2:1) samples. Moreover, we used Arg-free PAE as a control in different studies and found that the optimal PAE: alginate weight ratio for creating PAE/alginate (PA) particles was 1:1. The average hydrodynamic size of the optimized particles in various groups is provided in Figure 1E. Results demonstrated that the use of binary formulations of Arg-N-PAE with different ratios had a substantial effect on the size and zeta potential of particles, depending on the Arg: PAE weight ratio, while the polydispersity index (PDI) was calculated below 0.4. Since the PDI below 0.5 specifies the uniformity of all particles,[38] we would conclude that the APA particles were monodisperse. Moreover, while the diameters ranging from 269 to 334 nm were estimated for APA particles, PA particles had higher particle sizes (379 ± 112 nm) than APA particles ($P < 0.05$). It might be due to the hydrogen bond formation between Arg and alginate, which may affect the degree of cross-linking and the resulting particle size. Arg content also affected the surface charge of the Arg-N-PAE copolymers and their APA particles, potentially affecting their stability and aggregation behavior. After the APA particles formed, the zeta potentials were measured and found to be in the range of −11.3 to −6.5 mV (**Figure 1F** and Table S2, Supporting Information). When the zeta potentials of Arg-loaded particles varied from −5.8 to +4.6 mV due to the varying amounts of Arg and alginate on the particle surfaces. Previous studies also showed that the zeta potential of PAE with oligopeptide-modified termini/siRNA NPs could be changed by adjusting their PAE/siRNA ratio, enabling a range from negative to neutral or positive charges.[34] Our results indicate that reducing the ratio of anionic/cationic alginate: A3P formulations from 2:1 to 1:1 led to a significant reduction in average particle size to 286 nm, and a change in zeta potentials to a positive value of +4.6 mV. However, more decreases in the anionic/cationic alginate: A3P formulations to a 1:2 ratio reduced the stability of complexes and the inability to particle formation. According to the results summarized in Table S2 (Supporting Information), alterations in Arg: PAE ratio led to variations in the electrophoretic mobility and conductivity of the particles, indicating modifications in their surface characteristics. This feature could be valuable to control the cellular uptake of the particles.[39] Interestingly, increasing the Arg: PAE weight

© 2024 The Author(s). Advanced Therapeutics published by Wiley-VCH GmbH

23663987, 2024, 12, Downloaded from https://advanced.onlinelibrary.wiley.com/doi/10.1002/adtp.202400329 by Universitaet Bayreuth, Wiley Online Library on [14/03/2025]. See the Terms and Conditions (https://onlinelibrary.wiley.com/terms-and-conditions) on Wiley Online Library for rules of use; OA articles are governed by the applicable Creative Commons License

ratio to 1:3 led to a significant improvement in zeta potential. This improvement was attributed to the positively charged amino group of Arg, which interacted with the negatively charged carboxyl groups of alginate, resulting in higher zeta potential values. However, due to the steric effect, the incorporation of more Arg (A2PA particles) led to a slight decrease in the zeta potential to 0.9 ± 0.2 mV. Generally, the total positive charge of complexes is enhanced by increasing the positive Arg-N-PAE relative to the negative alginate in the formulations. However, results demonstrated that the zeta potential of APA particles was highly modulated by varying the Arg: PAE weight ratio, and the zeta potential of complexes did not exhibit a consistent trend. Complexes prepared with high Arg content copolymers (i.e., A2P and A3P) and alginate revealed a decrease in zeta potential values from positive to negative upon the increase of alginate in the formulation. However, zeta potential values of complexes prepared with A5P revealed a significant decrease but remained negative in different complex formulations. This variation in zeta potential can be related to the different packing distributions of alginate with Arg-N-PAE copolymers due to varying contents of the reactive amine groups of Arg available for interaction with alginate. This means that at high Arg content, the amine groups of Arg may affect the distribution of Arg-N-PAE chains in the particle structure, leaving Arg-N-PAE more exposed to the surface of the particles and resulting in positive zeta potential values. Confirmed by the DLS and zeta potential analysis, we can conclude that depending on their compositions, the resulting particles have a core-shell structure in A5PA and PA particle formulations. The alginate formed the shell and Arg-N-PAE created the core. Conversely, for the A3PA and A2PA samples, it is expected that alginate and Arg-N-PAE formed the core and shell, respectively, due to the positive charge of the particles. This structure may facilitate their interaction with cell membranes, which have a negative charge.

The core-shell structure formation of APA particles was further investigated using FTIR spectroscopy. Figure 1C shows that the alginate spectrum consisted of a carboxylate band at 1600 cm^{-1}, while the symmetric stretching vibration was observed at 1408 cm^{-1}. Moreover, the C—O—C stretching vibration of the glycosidic bond was identified in the region of 1000-1100 cm^{-1}. O—H stretching vibration of the hydroxyl groups and C—H stretching vibration related to the stretching vibration of the aliphatic groups were also observed between 3200–3500 and 2850–3000 cm^{-1}, respectively. Furthermore, the C—O—H bending vibration of the hydroxyl groups and the C—C stretching vibration of the aliphatic groups were observed in the region of 1300–1500 and 1000–1200 cm^{-1}, respectively.[40] After the formation of APA particles, Arg-N-PAE (AP) interacted with alginate through electrostatic interactions. The FTIR spectra of both A2PA and A5PA particles consisted of the characteristic bands of both alginate and Arg-N-PAE components with a right shift to lower wavenumbers, confirming the complex formation.[41]

The success of the transfection process relies on the creation of stable particles. Therefore, we conducted a study to investigate the impact of the Arg modification on the stability of the resulting APA particles for 24 h to optimize the most stable polymer formulation. In this regard, freshly prepared APA particles were incubated in phosphate buffer saline (PBS) for 24 h and the size and surface charges of particles were measured during this period. The results are displayed in Figure 1G and Figure S4 (Supporting Information) and show the low stability of the PA particles, confirming previous findings by Lynn et al.[42] The average dynamic size of the PA particles was measured to be larger than 800 nm after 12 h, confirming a high aggregation degree of particles or their swelling. In addition, an augmentation in particle size resulted in a rise in the surface charge to negative values (Figure S4, Supporting Information). However, the incorporation of Arg resulted in significantly stabilized particles for up to 12 h, and, then, the particle sizes were increased 1.2-2 times, depending on the Arg content. Moreover, the addition of Arg controlled the zeta potential to lower negative values (less than -8 mV after 24 h). Noticeably, our results revealed that the A3PA particle sizes were constant and below 330 nm with a zeta potential of ≈−1.1 mV up to 12 h, which was later increased to 550 nm with a zeta potential of −2.5 mV after 24 h. Arg has multiple functional groups that could contribute to hydrogen bonding with alginate, including amino groups, leading to stronger intermolecular interactions and greater particle stability. Therefore, the incorporation of Arg could provide extra crosslinking binding sites resulting in enhanced stability and decreased swelling ability of particles during the hydrophytic degradation. A similar observation was previously reported for other Arg-functionalized hydrogels.[43] In addition, Arg has a high pKa of guanidine groups in Arg-based components, which results in ionization only at acidic conditions.[44] Therefore, these Arg-loaded particles could have appropriate stability within a medium with a neutral pH (pH = 7.4). Furthermore, the lower zeta potential might be related to the swelling of particles and their degradation, leading to the removal of positively charged groups from the particle surface and a decrease in zeta potential.

The stability of APA particles strongly controlled the Arg release. Arginine's function in wound healing resembles a double-edged sword, where its concentration should be controlled spatially to improve wound healing while minimizing scar formation.[29] Having higher levels of Arg during the inflammation and initial stages of proliferation in wound healing can help prevent infection, promote angiogenesis, and aid in the formation of granulation tissue. On the other hand, lower levels of Arg during the later proliferation and tissue remodeling can reduce excessive collagen deposition and minimize the risk of developing nonfunctional scars.[45] Sakaguchi test was applied to investigate the estimation of the amounts of Arg released from the APA particles in the hydrolytic degradation process over 48 h in a physiological environment (PBS, pH = 7.4) (Figure 1H). Generally, a higher Arg-N-PAE: alginate weight ratio /higher Arg composition in APA particles resulted in a slower degradation rate. Notably, the release rate of Arg from A2PA, A3PA, and A5PA over 48 h was estimated at 67%, 55%, and 38%, respectively. Besides the importance of the release rate in wound healing, the total amount of Arg released locally was also critical. There were obvious differences in the Arg release between the first 24 h and the following day, probably due to differences in the amount of Arg loaded into the particles. Specifically, within the first 6 h, the total amount of Arg released from A2PA would likely be higher than that from A3PA and A5PA, indicating a higher local concentration of Arg at the wound site and less packing and complexation of particles. Despite experiencing Arg release at the initial hours, A3PA retained a significant amount within its particles due to its abundant Arg conjugation. In summary, the strategy of

© 2024 The Author(s). Advanced Therapeutics published by Wiley-VCH GmbH

23663987, 2024, 12, Downloaded from https://advanced.onlinelibrary.wiley.com/doi/10.1002/adtp.202400329 by Universitaet Bayreuth, Wiley Online Library on [14/03/2025]. See the Terms and Conditions (https://onlinelibrary.wiley.com/terms-and-conditions) on Wiley Online Library for rules of use; OA articles are governed by the applicable Creative Commons License

rational engineering of Arg-N-PAE offered the promise to modulate the Arg release profile in a controlled manner. In this system, the release of Arg from particles can be controlled by several factors, including the hydrolytic degradation process, which strongly depends on the crosslinking degree of alginate, particle compositions, and the pH and ionic strength of the surrounding environment. Alginate can form hydrogels through cross-linking with calcium ions, which could provide a network structure for complexation with the Arg-N-PAE. Especially, the composition of Arg-N-PAE could significantly influence the release rate of Arg from the particles. Previous studies also demonstrated that cargo release is achievable by integrating functional groups and employing PAE structures with modified hydrophilicity to regulate the hydrolytic degradation rate.[34]

2.2. Biophysical Characterization of Flii siRNA-APA Polyplex

After the formation of the APA particles, A3PA was chosen as a carrier for Flii siRNA. We applied self-assembly to create siRNA-laden particles. As shown in **Figure** 2A, the positively charged amine-terminated cationic Arg-N-PAE binds to negatively charged siRNA through electrostatic interactions and forms particles spontaneously due to strong amino-phosphate interactions. Next, alginate, a negatively charged polymer, was added to self-assemble onto the complex, leading to improved stability. However, the formation of particles was strongly dependent on the weight ratio of Arg-N-PAE/siRNA. To optimize this ratio for gene transfection, both A3PA and siRNA were incubated at different weight ratios (1/1, 10/1, 50/1, 100/1, and 200/1) to identify the ideal ratio to form complexes. In these complexes, Arg-N-PAE /siRNA ratio was 0.5/1, 5/1, 25/1, 50/1, and 100/1, respectively, since we applied weight ratio of 1:1 (w/w) Arg-N-PAE: alginate mixture. According to Figure 2B, varying the weight ratio of APA/siRNA altered the physicochemical properties of the formed complexes. Our results showed a gradual decrease in zeta potential and particle size with increasing A3PA/siRNA ratio in the formulation mixture from positive to negative values. At the APA/siRNA weight ratio of 1/1, the particle size was higher than pure APA particles (353 ± 117 nm versus 286 ± 28 nm) and the net surface charge was + 0.05± 0.02 mV. With increasing the APA/siRNA ratio upon 200/1, the net negative surface charge of the polyplexes enhanced to −39.0± 5 mV, and particle size reduced to 164 ± 12 nm. The negative surface charge at especially high APA/siRNA ratios (>50/1) could be consistent with our hypothesis on the formation of core-shell structure, where the Arg-N-PAE/ siRNA segment was part of the core, and the alginate portion formed the particle shells. In our study, we found that complexes with an APA/siRNA weight ratio of over 50/1 (specifically 100/1 and 200/1 weight ratios) had a negative charge. A weight ratio of 50/1 or higher was required for APA /siRNA complexes to have a particle size of less than 300 nm with low PDI (0.22-0.26). We also varied the ratio of APA/siRNA and used a NanoDrop UV–Vis Spectrophotometer to measure the amount of free siRNA. The siRNA loading efficiency in particles showed a rising trend as the weight ratio of APA to siRNA increased from 1/1 to 200/1 (Figure 2C). In addition, the RNA loading efficiency of particles at 100/1 and 200/1 was comparable to that of LIP which is a traditional carrier for siRNA. The siRNA-binding capacity of the developed A3PA was assessed using agarose gel electrophoresis at APA/siRNA ratios (w/w) of 10/1 and 100/1. Plain siRNA and siRNA-LIP were used as controls. To investigate the role of alginate on particle formation, this polyplex was similarly synthesized without alginate (siRNA-AP) at a polymer/siRNA weight ratio of 100/1. According to Figure 2D(i), compared to plain siRNA and LIP, APA particles loaded with siRNA (siRNA-APA) at a weight ratio of 100/1 showed the absence of any siRNA band, indicating the robustness of the complex. In contrast, when siRNA was complexed with APA (at a weight ratio of 10/1) and APA (at a weight ratio of 100/1) higher polymer-siRNA ratios were necessary to impede siRNA mobility. It could be related to the strong interaction between Arg or APA and siRNA at a weight ratio of 100/1. Therefore, we selected 100/1 as the optimized sample for the following experiments. At this ratio, according to the DLS analysis in Figure 2B, the unimodal size distribution with an average size of ≈239± 29 nm in PBS as a medium was formed. According to Figure 2A, we proposed that the creation of APA-siRNA polyplex involves the electrostatic interaction between siRNA and Arg-N-PAE, followed by the self-assembly of these components into tightly bound particles. Consequently, alginate interacted with remaining charged groups on the surface of the complex to form stable particles with negative surface charge. In this complex, the positively charged amino portions of Arg have the potential to create hydrogen bonds with the phosphate backbones of siRNA.[46,47] Consequently, when the Arg-N-PAE/ siRNA segment was mixed with anionic alginate, the higher affinity of the amino groups of Arg toward phosphate groups of siRNAs may imitate the distribution of Arg-N-PAE chains in the core of polyplex structure, leading to the formation of an alginate layer on the surface of polyplex and lower zeta potential values. Here, anionic alginate shielding of the cationic charge enhanced the stability of colloidal polyplex in the bloodstream. It could be related to the interactions with negatively charged serum proteins, potentially causing particle dissociation and siRNA release during circulation, thereby adversely affecting experimental outcomes. Previous studies also revealed that anionic polymers contributed to improved stability of the delivery complexes in biological systems while prolonging the integrity of siRNA once complexed in the particle and promoting transfection efficiency.[48] Next, we conducted an experiment to determine the ability of A3PA to protect siRNA from being degraded. In this regard, APA-loaded siRNA (siRNA-APA) and siRNA-LIP particles were exposed to various concentrations of heparin solution (1, 5, and 10 wt.%) as an electrostatic competition agent and used UV-Vis spectroscopy and Gel electrophoresis to determine the siRNA concentrations. In this treatment, siRNA was released in the heparin medium due to the decomplexation of the particles (Figure 2D(ii), F). The gel electrophoreses showed the absence of the siRNA band at low heparin concentrations (Figure 2D (ii)), however, at higher heparin concentrations (10 wt.%) some slight and faint lines were visible, which were negligible compared to those of siRNA-LIP particles. We concluded that the siRNA was completely encapsulated in the APA particles. UV–Vis spectroscopy revealed that compared to siRNA-LIP, siRNA-APA had a great protective effect even at high heparin concentrations (Figure 2F). It could be due to the strong amino-phosphate interactions between Arg and siRNA and the formation of the alginate shell.

© 2024 The Author(s). Advanced Therapeutics published by Wiley-VCH GmbH

23663987, 2024, 12, Downloaded from https://advanced.onlinelibrary.wiley.com/doi/10.1002/adtp.202400329 by Universitaet Bayreuth, Wiley Online Library on [14/03/2025]. See the Terms and Conditions (https://onlinelibrary.wiley.com/terms-and-conditions) on Wiley Online Library for rules of use; OA articles are governed by the applicable Creative Commons License

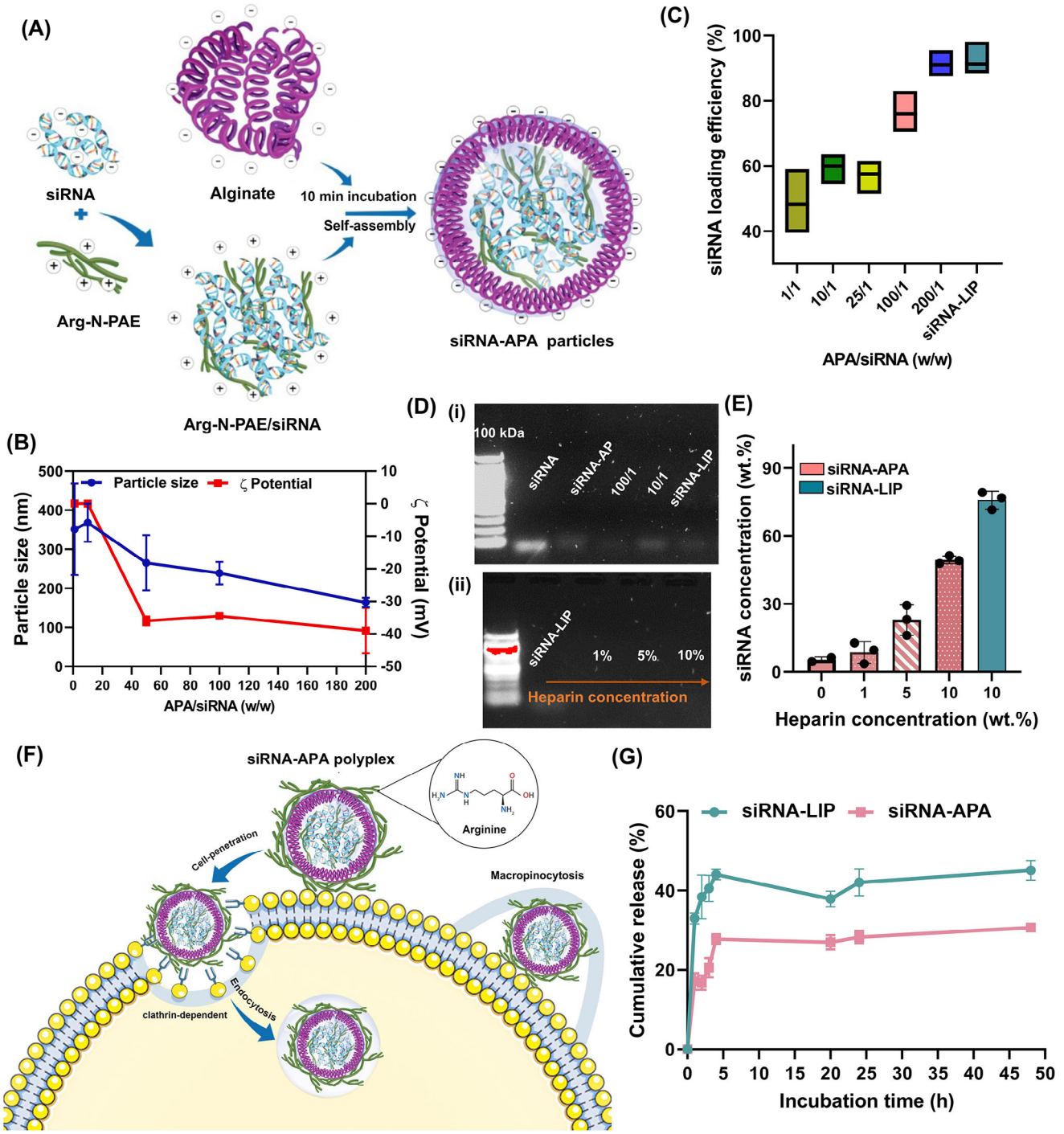

Figure 2. Biophysical characterization of siRNA-APA polyplex: A) Schematic illustration of the preparation of siRNA-APA polyplex via electrostatic-based self-assembly, B) Average hydrodynamic diameter and zeta potential values of siRNA-APA polyplexs as a function of APA/siRNA weight ratio, C) The siRNA loading efficiency of polyplexes, as a function of APA/siRNA weight ratio, D) Gel electrophoresis assay to study i) Gel retardation of siRNA at 2 different APA/siRNA ratios (100/1 and 10/1), in comparison to plain siRNA, siRNA-LIP, and siRNA-laden alginate-free particles (siRNA-AP) and to evaluate ii) stability of siRNA-APA polyplex in contact with various concentrations of heparin solution, compared to siRNA-LIP complex, E) Stability analysis of siRNA-APA polyplexes in contact with various concentrations of heparin solutions, in comparison to siRNA-LIP, F) The schematic representation of the cell membrane penetration of siRNA-APA polyplex with Arg as a shell. The interaction between side-chain amino groups of Arg on the surface of siRNA-APA polyplex and cell surface receptors including phosphate, sulfate, and carboxylate supports siRNA-APA polyplex translocation into the cytoplasm through endocytosis. G) The cumulative release of siRNA from siRNA-APA and siRNA-LIP in PBS solution (pH = 7.4) for 48 h. Results are presented as mean ($n \geq 3$) ± SD.

© 2024 The Author(s). Advanced Therapeutics published by Wiley-VCH GmbH

23663987, 2024, 12, Downloaded from https://advanced.onlinelibrary.wiley.com/doi/10.1002/adtp.202400329 by Universitaet Bayreuth, Wiley Online Library on [14/03/2025]. See the Terms and Conditions (https://onlinelibrary.wiley.com/terms-and-conditions) on Wiley Online Library for rules of use; OA articles are governed by the applicable Creative Commons License

The interaction between Flii siRNA and APA can be further studied in the context of gene therapy. Based on the mechanism proposed in Figure 2F, the Flii siRNA can be complexed with Arg-N-PAE and alginate to form particles. These particles can be delivered to target cells to silence the expression of Flii. Figure 2F and previous studies[32] illustrate the importance of Arg due to its positively charged amino groups,[46] which could form hydrogen bonds with anionic phosphate, sulfates, and carboxylate groups on cellular membranes. Following the formation of bidentate hydrogen-bonding interactions, the ion-pair dissociates on the inner side of the cell membrane after translocating across the membrane, which also supports the internalization of the siRNA-APA polyplex.[49] This approach can be used to treat various diseases that are associated with abnormal Flii expressions, such as chronic scar wounds. However, a sustained release of Flii siRNA is desired for efficient disease treatment. Delivery of siRNA to cells is a critical step in gene silencing experiments, as the efficiency of siRNA uptake could improve the effectiveness of the gene knockdown. Therefore, the release of siRNA from APA particles and LIP was studied using UV-Vis spectroscopy. Figure 2G exhibits the release of siRNA from polyplexes in PBS (pH = 7.4). The burst siRNA release was detected during the first 6 h in 2 different samples, and they showed different rates owing to the decomplexation of particles. In this regard, siRNA-LIP revealed a significantly higher release rate that could be related to the easier decomplexation, discussed in Figure 2D. For instance, after 2 h incubation of siRNA-LIP, 28% siRNA was released, which was 1.75 times higher than the released siRNA from siRNA-APA. The improved controlled release of siRNA in siRNA-APA polyplexes might be attributed to the strong electrostatic interaction of alginate with the cationic polymer (APA), the shielding role of alginate, and the condensation of siRNA in the core of polyplexes. This strategy could be more straightforward compared to other recent strategies to promote local siRNA release. For instance, Fliervoet et al.[50] developed polyplexes based on siRNA and poly(2-dimethylaminoethyl methacrylate) (PDMAEMA) and loaded it into a thermosensitive hydrogel to improve siRNA release. Our findings confirm that when siRNA interacts with Arg-N-PAE and the alginate shell, it leads to longer half-lives and reduced degradation. This ensures that the siRNA is released in a controlled manner as the polyplexes degrade.

2.3. BJ Fibroblast Responses Mediated by APA Particles

Before the evaluation of siRNA-APA /cell interactions, the cellular uptake of APA particles was analyzed using human skin BJ fibroblasts essential for wound healing. A primary strategy involved examining the potential toxicity of APA particles resulting from their released macromolecular components. Therefore, the BJ cells were exposed to varying concentrations of APA particles, spanning from 10 to 200 μg ml^{-1} to optimize the concentration of each group with the highest cytocompatibility. Alumarblue assay was conducted after 24 h incubation of particles, and the results were normalized compared to the control (TCP), in which cells have not been in contact with particles (**Figure 3A**). It was shown that the cells' metabolic activity at all concentrations of particles was measured to be above 80%, indicating that all particles supported the cell viability, and there was no cytotoxicity of particles toward BJ cells. However, when the concentration of APA particles increased to 100 μg ml^{-1}, the cell viability was slightly reduced. Accordingly, the optimized concentration for all groups was set at 50 μg ml^{-1}. As shown in Figures 3B and C, the viability of BJ fibroblasts treated with various concentrations and types of particles was assessed after 1 and 2 days of culture using a live-dead assay. Results showed that the cell viability in contact with APA particles was higher than 90% after 2 days of culture supporting that the particle concentration of 50 μg ml^{-1} is cytocompatible for BJ fibroblasts. Furthermore, it was evident that Arg loading increased cell viability. Moreover, with the prolongation of culture time to 2 days, no significant differences could be detected between the cells in the positive control and cells treated with particles, suggesting the suitability of the particles in skin tissue engineering application. Next, to assess the uptake of particles by BJ cells, they were incubated with APA particles at optimized concentrations for a duration of 6 and 24 h, and the cellular uptake was investigated using flow cytometry (Figure 3D, Figure S5, Supporting Information). Remarkably, the uptake of APA particles was enhanced with increasing Arg content. The highest cellular uptake was measured for A3PA particles, which was ≈2-fold higher than that of PA particles after 6 h and all other samples after 24 h of culture. However, the cellular uptake of both A2PA and A5PA was comparable during 24 h. This result showed a great correlation with the primarily measured zeta potential of particles since the particles with a slightly negative or positive zeta potential were often preferred for cellular uptake. The fluorescence microscopy image (Figure 3E) also confirmed the successful uptake of A3PA particles in BJ cells, which can be due to the interaction of Arg with cell surface receptors, such as integrins, involved in the internalization of particles. Arg may also help to promote the formation of endocytic vesicles, which could engulf and transport the particles into the cell. It has been reported that Arg could increase the expression of genes involved in endocytosis and intracellular trafficking,[51] which may contribute to its ability to accelerate APA particle uptake.

To investigate the impact of the released Arg from the APA particles on the migration of BJ cells, an in vitro scratch test was conducted. According to Figure S6 (Supporting Information), and Figures 3F and G, during the first 24 h incubation, many cells migrated into the scratch zone in various APA samples, however, a limited number of cells was visible in the scratched region of control and PA groups. The quantitative analysis on scratch closure (Figure 3F) after 48 h incubation showed enhanced degrees of closure in contact with A2PA, A3PA, and A5PA particles by ≈1.29, 1.3, and 1.2 folds, respectively, compared to PA ones. Studies have suggested that the released Arg could accelerate the gap closure of fibroblast monolayers by promoting cell migration and proliferation. One proposed mechanism is the potential of Arg in increasing the production of NO by the cells, which in turn can stimulate the migration of fibroblasts and other cells involved in tissue healing. Moreover, Arg could increase the expression of genes associated with cellular proliferation and extracellular matrix (ECM) synthesis, which may also contribute to accelerating the gap closure in fibroblast monolayers.[29] When a scratch is made on a fibroblast monolayer, the cells at the edge of the scratched region begin to migrate into the denuded area. This process is driven by the formation of lamellipodia. The lamellipodia extend into the wound

© 2024 The Author(s). Advanced Therapeutics published by Wiley-VCH GmbH

23663987, 2024, 12, Downloaded from https://advanced.onlinelibrary.wiley.com/doi/10.1002/adtp.202400329 by Universitaet Bayreuth, Wiley Online Library on [14/03/2025]. See the Terms and Conditions (https://onlinelibrary.wiley.com/terms-and-conditions) on Wiley Online Library for rules of use; OA articles are governed by the applicable Creative Commons License

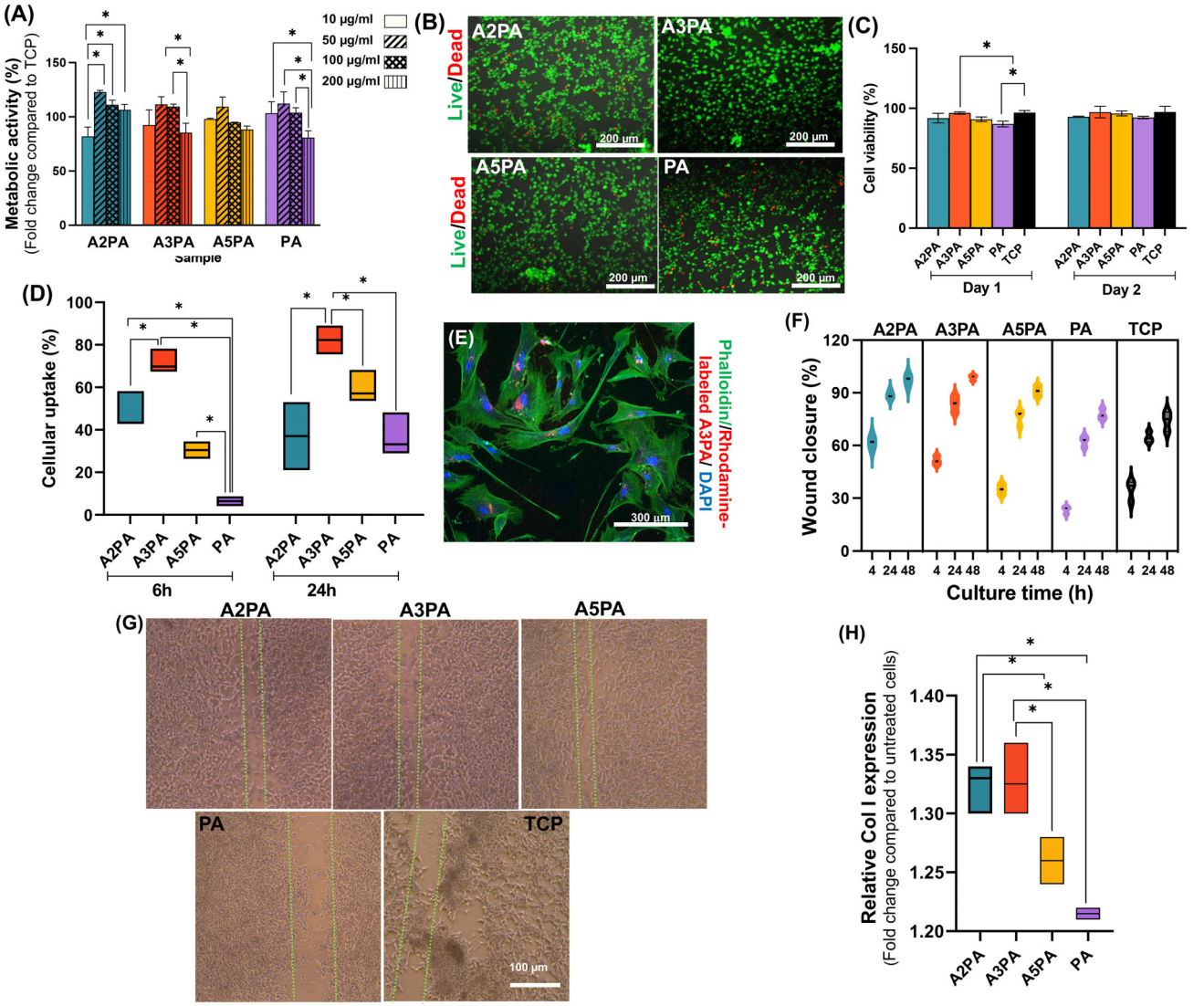

Figure 3. In vitro BJ fibroblast behavior mediated by APA particles: A) The effect of APA concentration on the metabolic activity of fibroblasts, assessed using Alamarblue™ assay, B and C) The viability of BJ fibroblasts after treatment with APA particles, determined using a live/dead assay: B) Representative fluorescent images of live/dead staining after incubation with APA particles for 2 days, and C) quantitative analysis of live and dead cells after 1 day of culture. BJ cells were stained with calcein-AM (green) and EthD-1(red) after incubation with various APA particles, D) Intracellular uptake of Rhodamine-labeled APA particles after 6 and 24 h of incubation. Transfected cells were evaluated by flow cytometry, and the percentage of cellular uptakes in various APA groups were compared to the control (untreated cells, TCP), E) Representative fluorescent image of intracellular uptake of Rhodamine-labeled A3PA particle by fibroblasts 6 h post-incubation. The red, blue, and green colors represent Rhodamine-labeled A3PA particles, cell nuclei, and cell F-actins, respectively. Scratch assay to evaluate wound healing capabilities measuring the BJ fibroblast migration after 4, 24, and 48 h toward the scratched area; The scratch closure is represented by F) the percentage of scratched surface area without cell coverage and G) representative bright-field images showing the coverage of scratch area as measured for wound healing after 48 h incubation with particles, H) The collagen I (Col I) expression level was measured using qPCR as a skin wound healing-related factor in BJ cells treated with various APA particles for 48 h and after the scratch test. Results are shown as the mean ($n = 3$) ± SD (*: statistical difference, $P < 0.05$).

area, attach to the ECM, and pull the cell body forward. This crawling movement is mediated by the stimulation of numerous signaling pathways, including the Rho family of small GTPases. As the cells migrate into the wound area, they also begin to proliferate, which contributes to the closure of the gap. In addition to cell migration and proliferation, the closure of the gap also involves ECM remodeling. The ECM is a complex network of proteins and glycosaminoglycans that provides structural support for cells. During the wound healing process, the ECM is remodeled by fibroblasts, which deposit new ECM proteins and break down old ones. This remodeling process helps to fill in the gap and restore the structural integrity of the tissue.[52] Moreover, fibroblasts are known to mainly contribute to synthesizing and depositing collagen type I (Col I) at the wound site. BJ cells could also metabolize Arg through arginase for the synthesis of collagen. Therefore, the gene expression at the

© 2024 The Author(s). Advanced Therapeutics published by Wiley-VCH GmbH

23663987, 2024, 12, Downloaded from https://advanced.onlinelibrary.wiley.com/doi/10.1002/adtp.202400329 by Universitaet Bayreuth, Wiley Online Library on [14/03/2025]. See the Terms and Conditions (https://onlinelibrary.wiley.com/terms-and-conditions) on Wiley Online Library for rules of use; OA articles are governed by the applicable Creative Commons License

transcriptional level was measured to investigate the potential impact of APA samples on the formation of fibrotic tissue during the wound healing process. According to Figure 3H, all samples revealed enhanced levels of Col I expression compared to untreated cells (control) after 24 h incubation. Interestingly, among the samples, A3PA and A2PA demonstrated a higher Col I expression than PA-treated cells owing to increased Arg release.

2.4. BJ Fibroblast Reactions Mediated by Flii siRNA-APA Polyplex

Next, we assessed the transfection efficiency of siRNA-APA particles in BJ fibroblast cells. Initially, we examined the metabolic activity of cells when exposed to the siRNA-APA complex, as compared to siRNA-LIP, siRNA, and A3PA particles. Our findings showed a consistent increase in metabolic activity over 2 days after treatment in various groups (**Figure** 4A). Notably, siRNA-APA could efficiently improve the growth and proliferation of BJ cells in vitro without inducing any cytotoxicity. Moreover, siRNA-APA and A3PA carriers exhibited superior siRNA transfection compared to plain siRNA and siRNA-LIP ($P < 0.05$) (Figure 4B). After confirming the targeting efficiency, we tested the delivery efficiency of siRNA targeted to BJ cells. In this regard, silencing efficiency was evaluated using fluorescence imaging. The fluorescent images in Figure 4C show that transfection of BJ cells with A3PA and siRNA effectively and specifically silenced red signals compared to the control (TCP, siRNA-LIP, A3PA, and siRNA). These results correlated with the high efficiency of complexation observed in the gel retardation assays. To acquire a deeper understanding of cellular responses following treatment with siRNA-APA polyplex, the expression of the Flii gene and wound healing-related gene (Col I) at the transcript level was determined in BJ cells using quantitative polymerase chain reaction (qPCR) (Figures 4D and E). Our results show a substantial upregulation of Col I gene expressions and downregulation of Flii gene expression relative to the control group, after treatment with siRNA-APA. Turner et al.[53] previously used thermally hydrocarbonized porous silicon NPs as a carrier for Flii siRNA, which were coated with chitosan and showed a 60% reduction in Flii RNA expression compared to controls, while it was not effective compared to Flii siRNA loaded with LIP. Our results also revealed the enhanced Col I expression in the A3PA group, which could be related to the effective role of Arg metabolized by fibroblasts to form ornithine, serving as a substrate material for the synthesis of collagen.[54] However, A3PA did not have a significant role in the Flii gene expression compared to the control. In other words, while plain siRNA was not effective in the expression of these genes, siRNA-LIP could only support the downregulation of Flii gene expression and did not show a significant role in the Flii gene expression. According to our results, A3PA efficiently delivered siRNA to BJ cells and knocked down endogenous gene expression at mRNA levels. In addition, Col I is one of the main components in the skin, and its production and deposition at the initial stages of wound healing could stimulate granulation tissue formation and accelerate re-epithelialization. According to Figure 4E, Flii knockdown using APA particles significantly increased BJ proliferation and Col I expression, suggesting the multifunctional role of siRNA-APA particles on both Arg and Flii Rh-siRNA release in the wound healing process. According to the potential involvement of Flii siRNA-APA particles in the knockdown of Flii expression and upregulation of Col I in the first days of cell interactions, it is expected that these polyplexes could be promising for chronic wound treatment.

Based on our results, A3PA polyplexes have emerged as a new candidate for gene delivery owing to their versatility, high transfection efficiency, and low toxicity. They are well-suited for delivering nucleotides to dermal fibroblasts and macrophages. It is noteworthy that PAE has been successfully used as a transfection agent for delivering siRNA, but this is the first study to examine its efficacy in combination with Arg and alginate for RNA delivery.

2.5. J774.1 Macrophage Response Mediated by APA Particles

The effect of the APA particles was also studied on the J774.1 macrophage function. To determine the role of APA formulations on macrophage function, LPS pre-treated cells were incubated with particles for a duration of 24 and 48 h. Figure S7A (Supporting Information) shows that before LPS pre-treatment, J774.1 cells (TCP, 0 h) revealed a round-shape morphology, confirming the cells are not activated (M0). On the contrary, when the macrophages were pre-treated with LPS, spindle-shaped cells appeared. This change in the morphology of cells after LPS pre-treatment was already reported in previous studies, confirming the activation of cells to the M1 phenotype.[55] **Figure** 5A, and Figure S7B (Supporting Information), demonstrated the high cell viability (more than 90%) for cells after LPS pre-treatment and incubation with APA particles, confirming that LPS pre-treatment did not have cytotoxic effects on the cells. For instance, after 2 days of culture, the cell viability in contact with the A3PA particles was 1.9 and 1.2 times higher than that of PA and TCP, respectively. Furthermore, as depicted in Figure 5B, APA particles were not only non-toxic in contact with J774.1 macrophages but also boosted cell proliferation compared to PA particles and TCP ($P < 0.05$). This could be attributed to the role of Arg, which could have provided a sustained supply of the amino acid to the cells, thereby increasing the viability of macrophages. As it is shown in the literature, Arg is greatly important for the metabolism of macrophages providing them with the energy and nutrients they need to carry out their functions. In addition, the morphology of cells after the treatment has changed, which was depending on the APA formulation. For instance, while spindle-like cells were still observed after treatment with PA particles, A3PA treatment completely changed them to round-shape morphology. This could be attributed to the change in the cell phenotype after APA treatment. According to previous studies, activated macrophages can produce reactive oxygen species, NO, and pro-inflammatory cytokines like tumor necrosis factor-α (TNF-α).[56] Therefore, to further study the role of APA on the cell phenotype, the nitrate/ NO level in the medium was determined, since it is directly related to the cell activity and phenotype. The nitrate/ NO release study in Figure 5C shows the potential of APA-induced nitrate production in J774.1 cells. To stimulate nitrate production, the cells were pre-treated with LPS, before incubation with APA particles. Results showed that the amount of produced nitrate has been significantly enhanced after LPS treatment of control (TCP) cells (TCP versus TCP (LPS)), confirming

© 2024 The Author(s). Advanced Therapeutics published by Wiley-VCH GmbH

23663987, 2024, 12, Downloaded from https://advanced.onlinelibrary.wiley.com/doi/10.1002/adtp.202400329 by Universitaet Bayreuth, Wiley Online Library on [14/03/2025]. See the Terms and Conditions (https://onlinelibrary.wiley.com/terms-and-conditions) on Wiley Online Library for rules of use; OA articles are governed by the applicable Creative Commons License

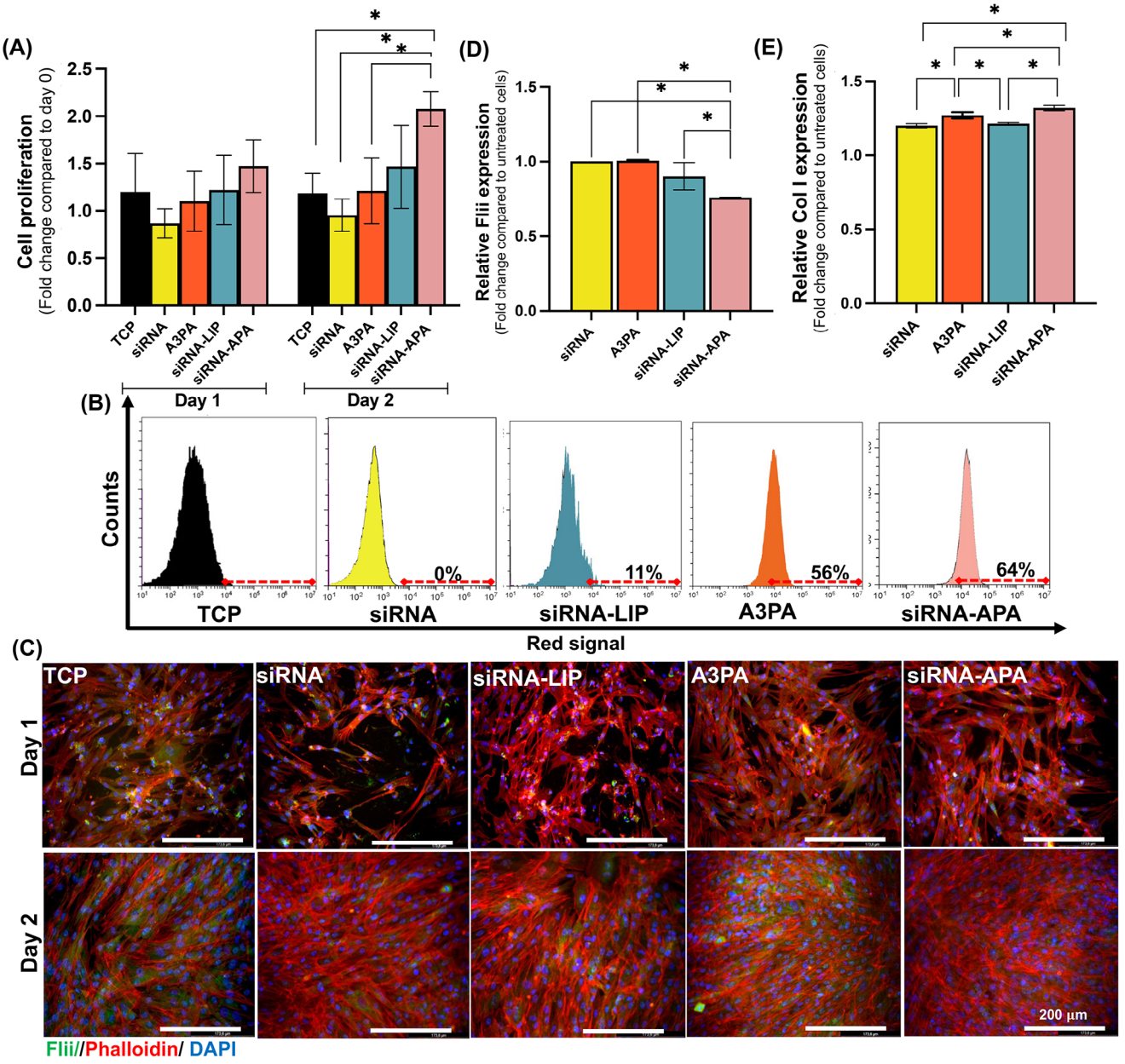

Figure 4. Flii siRNA transfection and BJ fibroblast interaction with A3PA polyplex: A) Proliferation of BJ fibroblasts treated with siRNA-APA and siRNA-LIP polyplexes, plain siRNA, A3PA and control (TCP), determined using Alamarblue™ assay, B) Cellular uptake of Flii Rh-siRNA using various carriers and controls (TCP, A3PA, and plain siRNA), C) Representative fluorescent microscope images monitoring the transfection of Flii Rh-siRNA using siRNA-APA, in comparison with untreated cells (TCP), siRNA-LIP (positive control), and A3PA in BJ fibroblasts 24 h post-incubation. The red, blue, and green colors represent F-actin, cell nuclei, and Flii, respectively. Relative gene expression of D) Flii and E) Col I was conducted after 24 h post-incubation. The gene expression levels were normalized to untreated cells devoid of any treatment, with CypA serving as the housekeeping gene. Data are presented as mean (n = 3) ± SD (*$p < 0.05$).

the change in the macrophage phenotype. Moreover, nitrate production increased following LPS pre-treatment and incubation with APA, depending on the particle formulation. Notably, the concentration of released nitrate increased to 3.5 ± 0.5 µM and 3.3 ± 1.2 µM after incubation with A2PA and A3PA, respectively. This was significantly higher than that in contact with A5PA (6-fold), PA (13-fold), and control (TCP, 22-fold), and even higher than the macrophages treated with LPS (TCP (LPS), 2.5-fold) after 24 h incubation ($P < 0.05$). This could be related to the role of Arg in the modulation of nitrate/ NO levels. Arg is a crucial nutrient for macrophages as it is a precursor for the production of nitrate. Generally, Arg released from particles can be metabolized by cells in 2 ways: 1) nitrate/ NO production, and 2) it can be used for collagen synthesis via ornithine metabolism. After macrophage activation using LPS, macrophages become activated to M1 during the inflammation phase of the wound healing

© 2024 The Author(s). Advanced Therapeutics published by Wiley-VCH GmbH

23663987, 2024, 12, Downloaded from https://advanced.onlinelibrary.wiley.com/doi/10.1002/adtp.202400329 by Universitaet Bayreuth, Wiley Online Library on [14/03/2025]. See the Terms and Conditions (https://onlinelibrary.wiley.com/terms-and-conditions) on Wiley Online Library for rules of use; OA articles are governed by the applicable Creative Commons License

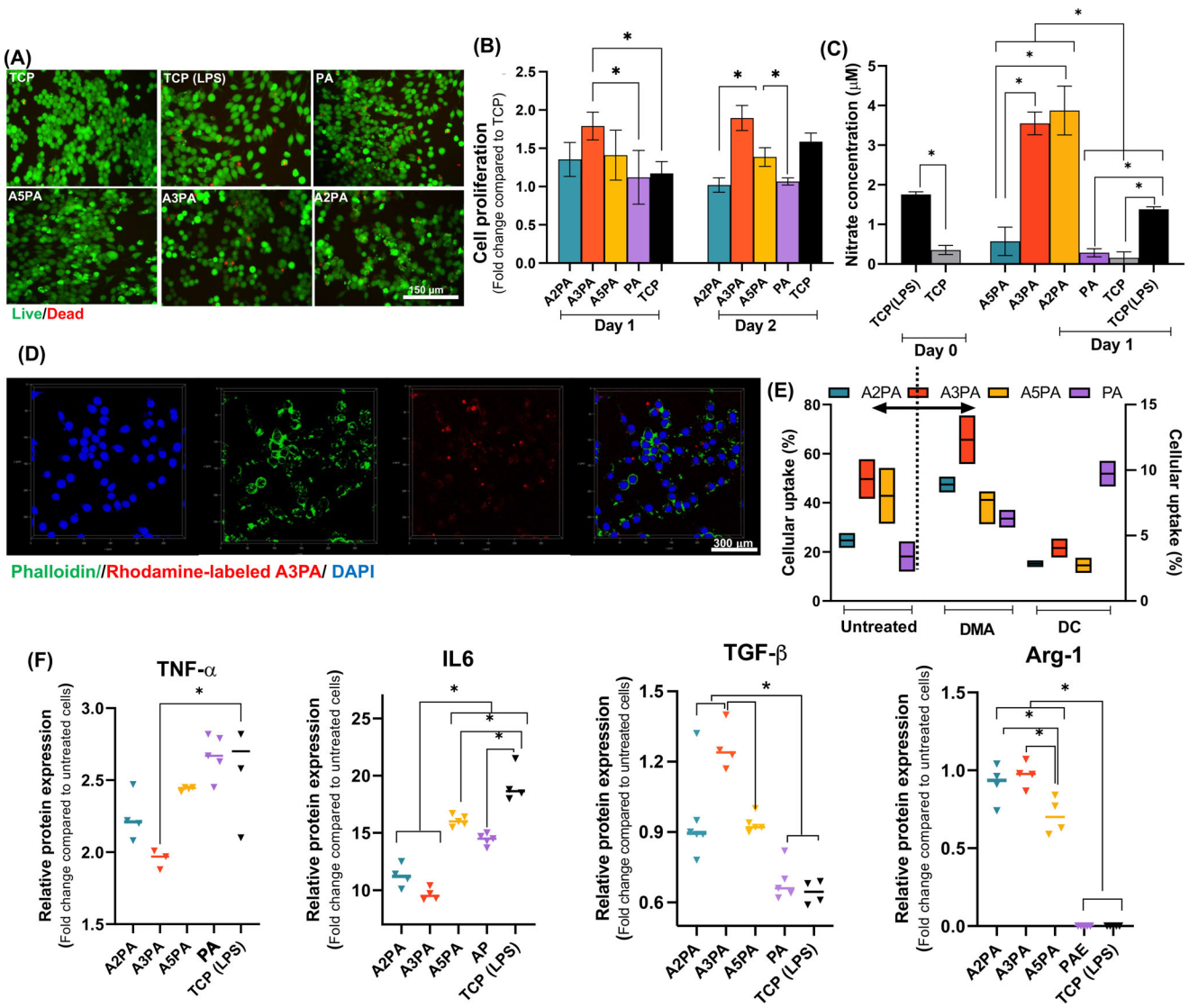

Figure 5. In vitro J774.1 macrophage behavior mediated by APA particles: A) The role of APA formulation on the viability of macrophages after LPS pre-treatment; Fluorescent images show the presence of live (green) and dead (red) cells stained with calcein-AM and EthD-1, respectively, B) The role of APA concentration on the proliferation of macrophages over 2 days of culture, determined using Alamarblue™ assay, C) The NO production before and after 24 h incubation of LPS-pretreated cells with various APA formulations, D) Representative confocal microscopy images of Rhodamine-labeled A3PA particles uptaken by macrophages 24 h post-incubation. The red, blue, and green colors represent Rhodamine-labeled A3PA particles, cell nuclei, and cell F-actins, respectively, E) Uptake of APA particles by macrophages, after 6 h incubation. Before APA treatment, the cells were incubated with 2 endocytic inhibitors. The inhibitors DC, and DMA were used to investigate the uptake mechanism, compared to untreated cells. Transfected cells were evaluated using flow cytometry, and the uptake percentage of particles was determined compared to the control (TCP) in each group. Dash lines and arrows represent the y-axis to determine the cell for each group, F) in vitro macrophage repolarization; qPCR analysis of TNF-α and IL6 relative gene expression levels as M1 markers and TGF-β and Arg-1 relative gene expression levels as M2 markers conducted 24 h post-incubation. The gene expression levels were normalized to untreated cells that did not receive any treatment. GAPDH was used as a housekeeping gene. Data are represented as mean (n = 3) ± SD (*$p < 0.05$).

process and serve L-Arg, which serves as the substrate for iNOS, resulting in the production of NO. The NO production induced by biomaterials is similarly reported for other types of biomaterials including glycidyl methacrylate-modified chitosan (CS-GMA), GMA- chitosan/Arg-poly(ester amide), and Arg-based poly (ester urea urethane) and glycidyl methacrylate-modified chitosan.[43] It has been reported that the NO derived from Arg can endorse the wound healing process by hindering infection, improving angiogenesis, and facilitating re-epithelialization.[57] However, the random and unregulated release of biological signals such as NO might result in adverse effects on the healing of wounds. For instance, NO has a cytostatic effect in high concentrations, which may hinder cellular ornithine-decarboxylase activity, leading to reduced cell proliferation.[58] Our results demonstrated that, depending on the desired NO concentration, APA composition could be tuned to provide appropriate cell responses.

© 2024 The Author(s). Advanced Therapeutics published by Wiley-VCH GmbH

23663987, 2024, 12, Downloaded from https://advanced.onlinelibrary.wiley.com/doi/10.1002/adtp.202400329 by Universitaet Bayreuth, Wiley Online Library on [14/03/2025]. See the Terms and Conditions (https://onlinelibrary.wiley.com/terms-and-conditions) on Wiley Online Library for rules of use; OA articles are governed by the applicable Creative Commons License

In the next step, the uptake of J774.1 cells was analyzed using flow cytometry after transfecting them with APA particles and comparing them with PA particles for 6 and 24 h (Figure S8, Supporting Information). It can be seen that the overall cellular uptake increased time-dependently. Moreover, our results also confirmed that after 6 h of incubation, cells internalized all particles, where 50–80% of the cell population showed internalized particles varying with the Arg content. The cell internalization enhanced to 90% after 24 h of incubation, suggesting the energy-dependent uptake. Moreover, after treatments with APA particles for 24 h, cells revealed a noticeable right shift upon cytometric analysis, proposing higher cellular uptakes of particles. However, the interaction between PAE and Arg improved the transfection efficiency of the APA particles, enhanced the cellular uptake of the particles, and promoted endosomal escape. Between the particles, PA and A5PA particles revealed less cell internalization after 24 h, indicating the negative surface charge of particles might be the reason for reduced cell internalization. In contrast, the higher internalization of A3PA particles than that of other modified particles introduces this composition as a promising candidate for gene and drug delivery vehicles. Confocal laser scanning microscopy image of J774.1 cells after 6 h of incubation with A3PA particles (Figure 5D) also showed diffused Rhodamine-labeled-particle signals throughout the cytosol, suggesting that A3PA effectively avoids degradative endo-lysosomes to permit cytosolic protein delivery.

To examine how the internalization pathway of particles is affected by the amount of Arg present in each particle composition, experiments were carried out using J774.1 cells incubated for 6 h with particles. The cells were pre-treated with two endocytic inhibitors named dansylcadaverine (DC) an inhibitor of clathrin-mediated endocytosis and dimethyl-amiloride (DMA) an inhibitor of macropinocytosis, before being incubated with particles. The uptake of the particles was then assessed using flow cytometry and the results are provided in Figure 5E. Generally, the uptake of particles in cells could occur through multiple mechanisms, including clathrin-mediated, receptor-mediated, and caveolae-mediated endocytosis, and macropinocytosis. The precise mechanism is dependent on the particle size and the surface properties of particles. Receptor-mediated endocytosis is a highly specific process, whereby ligands bind to specific cell surface receptors and trigger the internalization of the ligand-receptor complex.[59] In addition, clathrin-mediated endocytosis is a thoroughly understood mechanism wherein the clathrin-coated vesicles are formed to transport molecules from the cell surface to the endosomes. Caveolae-mediated endocytosis is a similar process to clathrin-mediated endocytosis, but it involves the formation of caveolae, which are specialized lipid rafts on the cell surface.[60] According to Figure 5E, in comparison to untreated cells, the presence of the macropinocytosis inhibitor (DMA) led to a reduced internalization of PA particles, as opposed to the clathrin-mediated endocytosis inhibitor (DC). It shows that PA was internalized primarily by macropinocytosis. This result was similarly reported for other types of PAE-based particles.[61] On the contrary, by loading particles with varying levels of Arg content and treating the cells with DC, the percentage of cells uptaking the Arg-loaded particles decreased, suggesting that clathrin-mediated endocytosis predominates as the main uptake mechanism. Noticeably, A3PA particle internalization was significantly hindered (4%) after DC treatment of cells and 6h incubation with particles, while following DMA incubation, the internalization was less pronounced after 6 h (12%). This observation of moderately decreasing numbers of cells uptaking APA particles compared to that with DC indicated that macropinocytosis played a minor role while clathrin-mediated endocytosis is the predominant mechanism in the uptake process. However, in the case of A5PA, the role of clathrin-mediated endocytosis and macropinocytosis was comparable, while the number of cells was significantly reduced compared to unloaded inhibitors. Figure 5E shows that compared to untreated samples (without inhibitors), three different mechanisms were identified differing in particle internalization. The primary group contained PA particles, showing a slight decrease in cellular uptake when exposed to DC and a higher uptaking decrease in the presence of DMA suggesting that macropinocytosis was the predominant route of PA particle uptake, while clathrin-mediated endocytosis played a medium role. The second group was based on A5PA, in which both uptake mechanisms had the same contribution to the cellular uptake. The last group represented A2PA and A3PA particles internalized by most of the macrophages. Here, the uptake was significantly hindered in the presence of DC, while inhibition of uptake was relatively moderate in the presence of DMA, showing a minor role in macropinocytosis. Our results demonstrated the importance of the PAE: Arg ratio on the cellular uptake initiated from the role of Arg as a cell-penetrating peptide (CPP) interacting with various receptors on the cell membrane. In summary, the APA on the surface of particles such as A3PA and A2PA could provide a positively charged surface for interaction with negatively charged cell surface receptors, facilitating particle internalization. Especially, the AP amino ester on the surface of the particles could interact with the clathrin protein on the cell surface, which could facilitate the formation of clathrin-coated vesicles and the internalization of the particles.

We identified that the APA particles possessed anti-inflammatory and immunomodulatory characteristics. Macrophages can be categorized into two primary phenotypes: M1 and M2. M1 macrophages contribute to the initial inflammatory response and produce pro-inflammatory cytokines. M2 macrophages participate in the later stages of inflammation and produce anti-inflammatory cytokines. Transitioning from M1 to M2 macrophages is essential for resolving inflammation and facilitating tissue healing. In this study, the regulatory effects of APA particles on the expression of genes involved in immune function, including arginase 1 (Arg-1), interleukin 6 (IL6), transforming growth factor-beta (TGF-β), and tumor necrosis factor-alpha (TNF-α), were investigated and are presented in Figure 5F. Our results revealed that after incubation of the control group (TCP) with LPS (TCP (LPS)), cells revealed a high level of inflammatory mediators including TNF-α and IL6 as reported in previous studies.[62] This result could confirm the change in the morphology of cells after LPS treatment (Figure S7A, Supporting Information). After incubation with PA particles, macrophages secreted higher levels of TNF-α and IL6, compared to cells in contact with the APA particles. The APA particles, depending on their Arg content, caused a considerably decreased release of inflammatory cytokines (IL6 and TNF-α) in macrophages. It could be related to the effective role of Arg to enhance NO release. According to Figure 5C,

© 2024 The Author(s). Advanced Therapeutics published by Wiley-VCH GmbH

23663987, 2024, 12, Downloaded from https://advanced.onlinelibrary.wiley.com/doi/10.1002/adtp.202400329 by Universitaet Bayreuth, Wiley Online Library on [14/03/2025]. See the Terms and Conditions (https://onlinelibrary.wiley.com/terms-and-conditions) on Wiley Online Library for rules of use; OA articles are governed by the applicable Creative Commons License

APA particles induced 2.5-13 folds with higher NO production in the cells than in ones cultured in TCP and transfected with LPS (TCP(LPS)) and/or AP. NO can act as a mediator of the polarization from M1 to M2 macrophages by preventing the creation of pro-inflammatory cytokines and stimulating the release of anti-inflammatory cytokines. For instance, NO can inhibit the NF-κB pathway (Nuclear factor kappa-light-chain-enhancer of activated B cells), which is involved in the production of pro-inflammatory cytokines by M1 macrophages.[63] On the other hand, NO can also activate the PI3K/Akt pathway, which plays a role in the production of anti-inflammatory cytokines by M2 macrophages.[64] In our study, we also looked at the macrophage polarization following treatment with APA particles by measuring the expression levels of Arg-1 and TGF-β (M2, anti-inflammatory markers). Arg-1 is an enzyme that metabolizes Arg and is concerned with immune function regulation. The upregulation of Arg-1 could result in a shift in macrophage polarization toward an M2 phenotype, involved in tissue regeneration and resolution of inflammation.[65] In addition, TGF-β plays a role in regulating the function of immune cells and promoting immune tolerance.[66] Notably, the findings showed a 12-fold increase in Arg-1 expression and a 2.4-fold increase in TGF-β expression after transfection with A3PA particles compared to the control (TCP(LPS)). These results confirmed the polarization of M1-induced macrophages into the M2-anti-inflammatory phenotype upon A3PA treatment. In summary, our data confirmed that it has a direct immunoregulatory effect on macrophages and has the potential to reduce pro-inflammatory functions in these cells, which are crucial features for wound healing. Therefore, the A3PA formulation was utilized as a carrier for Flii siRNA in the following section.

2.6. J774.1 Macrophage Response Mediated by Flii siRNA-APA Polyplex

To evaluate the transfection efficiency of siRNA-APA particles, we transfected J774.1 cells with siRNA-APA polyplexes, along with plain siRNA, A3PA, and siRNA-LIP. Untreated cells were also studied as control (TCP). At first, the cytotoxicity of siRNA-loaded polyplexes was studied using an Alamarblue assay for 2 days. The macrophages, compared to day 0, showed high metabolic activity after 2 days of culture in all groups (**Figure** 6A). However, the cell proliferation was tuned depending on the sample type. Noticeably, following 2 days of culture, the cell numbers (correlated with their metabolic activity) treated with siRNA-APA increased 2.3 times, compared to day 0, which was considerably higher than the activity of cells in contact with the siRNA-LIP (1.5 times) and siRNA (1.3 times). These results confirmed that APA particles were safer platforms for siRNA delivery. According to our results, siRNA-APA particles not only did not negatively impact cell viability compared to control but also increased cell proliferation. Furthermore, cell transfection was studied using fluorescent imaging and flow cytometry after treatment with siRNA-APA polyplexes, along with plain siRNA, A3PA, and siRNA-LIP particles. The Rhodamine-labeled siRNA was first produced and used to indicate the siRNA-based complexes. Rhodamine microscopically was detected in J774.1 macrophage (Figure 6B) before further quantification using flow cytometry (Figures 6C and D). Microscopic images taken from Rhodamine-labeled siRNA complexes (siRNA-APA) demonstrated that, compared to the images taken from cells in the control groups (siRNA-LIP and plain siRNA), the red signals in the cytoplasm of macrophages were significantly stronger indicating that these particles were effectively internalized by macrophages (Figure 6B). The images were in good accordance with the flow cytometry results (Figures 6C and D). The transfection efficiency varied significantly depending on the complex formulation. Nearly 89% of positively transfected cells could uptake siRNA-APA, similar to the A3PA samples an uptake which was significantly higher (1.2 times) than the cellular uptake of siRNA-LIP (control). The improved cellular uptake compared to the commercialized carriers was similarly reported for other amino acid-terminated PAE carriers.[34] These results confirmed the effective role of alginate in improving particle encapsulation efficiency with lower endosomal escape capacity and increased net surface charge. He et al.[67] previously reported the improved cellular uptake of NPs with higher surface charge (either positive or negative) than neutral particles signifying the crucial role of electrostatic interaction in the phagocytosis capability of macrophages. Other studies[68] also confirmed that polymers with negative surface charge could amplify oligonucleotide encapsulation, successfully support cellular membrane crossing, and simplify endosomal escape in fibroblasts and macrophages. Moreover, it has been reported that the combination of cationic/anionic PAE formulations could result in improved uptake of different types of cells, such as CT-2A murine glioma and B16-F10 murine melanoma.[61]

To study if siRNA expression in J774.1 macrophages could repolarize macrophages from M1 to M2 phenotypes, anti- and pro-inflammatory gene expression levels in M1 macrophages transfected with siRNA-APA, in comparison with A3PA, siRNA-LIP, and plain siRNA were measured after culture for 24 and 48 h (Figure 6E–H). Before transfection, all cells were stimulated to attain the M1 phenotype through incubation with LPS to mimic a pro-inflammatory activation similar to the wound environment. LPS stimulation increased pro-inflammatory gene expression levels measured using qPCR (i.e., TNF-α (2.8-fold) and IL6 (18.7-fold)) compared to untreated cells, which confirmed the M1 phenotype (Figure 6E and F). Compared to the control, pro-inflammatory cytokines (IL6 and TNF-αa) were gradually decreased, and anti-inflammatory cytokines (TGF-β, Arg-1) were gradually increased in the groups treated with APA particles ($P < 0.05$), indicating that all groups could control inflammation and improve the local microenvironment to some extent. Noticeably, the M1-induced cells incubated with siRNA-APA and siRNA-LIP showed a significant reduction in the expression of pro-inflammatory genes. For instance, cells treated with siRNA-APA and siRNA-LIP, compared to untreated cells, revealed decreased expression of TNF-α levels to 1.56-fold and 1.33-fold, respectively. In addition, the transfection of M1 cells with siRNA-APA also significantly improved anti-inflammatory gene (TGF-β, Arg-1) expression compared to transfected cells with A3PA, siRNA, and siRNA-LIP ($P < 0.05$) (Figures 6G and H). Noticeably, after 2 days of incubation of cells treated with siRNA-APA, compared to untreated cells, the enhanced expression level of Arg-1 to 2.2-fold was measured, which was notably higher than the expression levels in cells treated with A3PA (0.8-fold) and siRNA-LIP (1.4-fold). Accordingly, the results confirmed that J774.1 macrophages

© 2024 The Author(s). Advanced Therapeutics published by Wiley-VCH GmbH

23663987, 2024, 12, Downloaded from https://advanced.onlinelibrary.wiley.com/doi/10.1002/adtp.202400329 by Universitaet Bayreuth, Wiley Online Library on [14/03/2025]. See the Terms and Conditions (https://onlinelibrary.wiley.com/terms-and-conditions) on Wiley Online Library for rules of use; OA articles are governed by the applicable Creative Commons License

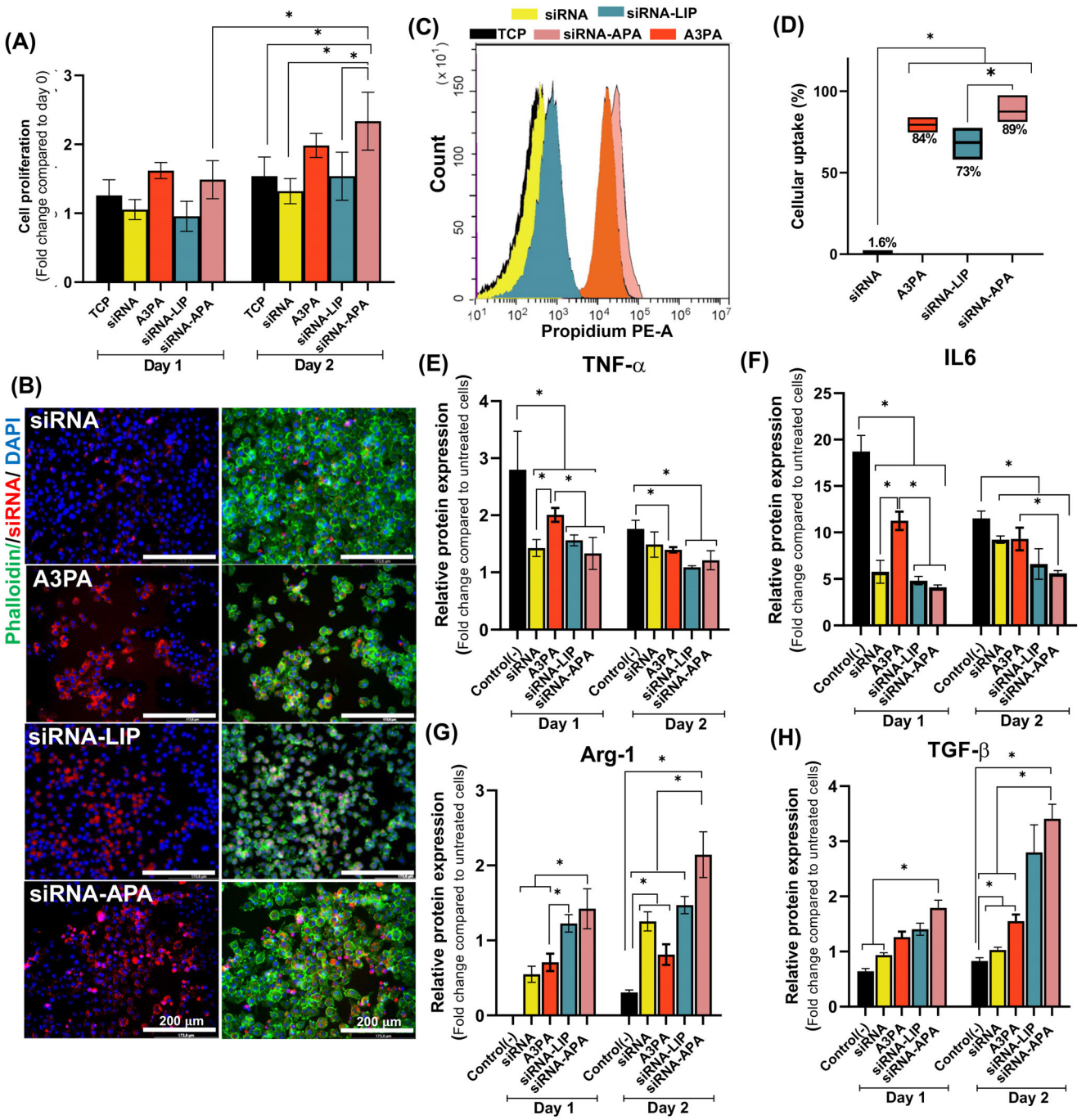

Figure 6. siRNA transfection and J774.1 macrophage repolarization studies using APA polyplex: A) Normalized proliferation of macrophages treated with siRNA-A3PA and siRNA-LIP polyplexes, plain siRNA, A3PA, compared to the control (TCP), determined using the Alamarblue assay, after 1 and 2 days of culture, B) Fluorescent microscope images monitoring the transfection of Flii Rh-siRNA released from polyplexes, A3PA, and siRNA in J774.1 macrophage 24 h post-incubation. The red, blue, and green colors represent Flii Rh-siRNA, cell nuclei, and cell cytoskeleton, respectively, C and D) Cellular uptake of Rh-siRNA using various carriers and controls (TCP, A3PA, and plain siRNA), E–H) in vitro macrophage repolarization: Relative expression analysis of E) TNF-α, F) IL6 as M1 phenotype markers, G) Arg-1 and, H) TGF-β as M2 phenotype markers conducted 24 and 48 h post-incubation. The gene expression levels were normalized to untreated cells that served as the control group. GAPDH was employed as a housekeeping gene for normalization purposes. Data are presented as mean (n = 3) ± SD (*$p < 0.05$).

© 2024 The Author(s). Advanced Therapeutics published by Wiley-VCH GmbH

23663987, 2024, 12, Downloaded from https://advanced.onlinelibrary.wiley.com/doi/10.1002/adtp.202400329 by Universitaet Bayreuth, Wiley Online Library on [14/03/2025]. See the Terms and Conditions (https://onlinelibrary.wiley.com/terms-and-conditions) on Wiley Online Library for rules of use; OA articles are governed by the applicable Creative Commons License

were efficiently repolarized from M1 to M2 after treatment with A3PA particles containing siRNA, confirming that these particles could effectively defeat the inflammation caused by LPS in J774.1 macrophages, which may accelerate the healing of chronic wounds more efficiently.

3. Conclusion

With this work, we have introduced a straightforward and effective formulation using L-Arg functionalized PAE (Arg-N-PAE) and alginate (APA) particles to promote the function and specificity and to control the toxicity of siRNA. APA formulations with 1:3 Arg: PAE and 1:1 Arg-N-PAE/Alginate were considered as optimized formulations based on their average particle size, zeta potential, Arg content, and its release, NO production, in vitro cell proliferation, cellular uptake, and immunomodulatory properties. The combination of Arg-N-PAE and anionic alginate admitted preserving the essential properties for in vitro gene silencing, including siRNA condensation, cellular uptake, and endosomal escape, while intensifying the biophysical characteristics of particles, including size, surface charge, and stability. As a consequence, APA particles could successfully transfect macrophages and downregulate the expression of pro-inflammatory genes while enhancing the expression of anti-inflammatory genes, leading to significant immunomodulatory properties. In other words, the successful delivery of siRNA to BJ fibroblasts and their transfection resulted in the downregulation of Flii gene expression and upregulation of Col I gene expression. In summary, this study demonstrates the feasibility of using a cocktail polyplex of APA to spatially deliver Arg and Flii siRNA to reprogram macrophages, highlighting their potential for chronic wound healing applications. Future studies will focus on evaluating the efficacy of this approach in vivo and optimizing the formulation for clinical translation. Moreover, the versatility of APA polyplexes will enable the development of new characteristics for innovative wound dressing platforms through further modifications of the hydrogel matrices.

4. Experimental Section

Materials: L-Arginine (Arg, ≥99%, Carl Roth), sodium alginate (Carl Roth), 1,4-Butanediol diacrylate (Sigma), N, N-Dimethylethylendiamin (Sigma), dichloromethane (DCM, Merck), diethyl ether (Merck), *N*-hydroxysuccinimide (NHS, Sigma–Aldrich), 1-(3-Dimethylaminopropyl)−3-ethyl carbodiimide hydrochloride (EDC, Cabosynth), 5(6)-carboxyfluorescein-N-hydroxysuccinimidester (Thermo Fisher) and 4-morpholinoethanesulfonic acid (MES buffer, Sigma) were used to synthesize APA particles. Dialysis tubes with molecular weight cutoff 6–8 and 12–14 kDa were acquired from Thermo Fisher Scientific. Sodium hydroxide (NaOH, Labochem), α-Naphthol (Sigma Aldrich), and urea (Carl Roth) were used in the Sakaguchi test. The Rhodamine-labeled Flii siRNA with sequences of GCUGGAACACUUGUCUGUGUU and CACAGACAAGUGUUCCAGCUU (Flii Rh-siRNA)) was purchased from Qiagen. Lipofectamine 2000 transfection (LIP, Invitrogen) was purchased as the commercial siRNA carrier. For siRNA-loaded particle characterization, heparin sodium (Sigma–Aldrich), SYBR Safe DNA Gel Stain (Invitrogen), agarose (Carl Roth), Opti-Minimal Essential Medium (MEM) reduced-serum medium (Minimal Essential Medium, Thermofisher), and sterile nuclease-free diethylpyrocarbonate (DEPC) water (Invitrogen) were purchased. For cell interaction evaluation, Dulbecco's Modified Eagle's Medium (DMEM, BioSell), Eagle's minimum essential medium (EMEM, ATCC), fetal bovine serum (FBS, BioSell), 10x Trypsin-EDTA (Gibco), penicillin–streptomycin (Pen/Strep, Gibco), GlutaMax (Thermo Fisher Scientific), Gentamycin-Sulfate (Sigma–Aldrich), 2- [4- (2-hydroxyethyl) piperazin-1-yl]ethanesulfonic acid (HEPES, Thermo Fisher Scientific), Triton 100x (Sigma–Aldrich), Dulbecco's Phosphate Buffered Saline (DPBS, Sigma), formaldehyde (PFA, Carl Roth), Alexa Fluor 488 Phalloidin (Invitrogen), Phalloidin Tetramethylrhodamine B isothiocyanate (Rhodamine phalloidin, Sigma), 4′,6-diamidino-2-phenylindole (DAPI, Sigma–Aldrich), bovine serum albumin (BSA, Sigma–Aldrich), lipopolysaccharide (LPS, Med Chem Express (MCE)), dansylcadaverine (DC, Sigma), dimethyl-amiloride (DMA, Sigma), Flii Polyclonal Antibody (Invitrogen) and Alexa Fluor 488 goat anti-rabbit IgG SFX kit Thermofisher, A31627) were provided. Moreover, Alamarblue Cell Viability Kit (Promega), Live/Dead Viability Kit (Calcein AM-Ethidium Homodimer-1 (EthD-1), Invitrogen), and Nitrite Assay Kit (Griess Reagent, Sigma–Aldrich), were purchased. For qPCR analysis, the RevertAid First Strand cDNA Synthesis Kit (Thermofisher) and innuMIX qPCR DSGreen Standard (Analytik Jena) were purchased. The list of primers purchased from BioRad was also provided in Table S1 (Supporting Information).

Formation of Arg-N-PAE/Alginate (APA) Particles: *Synthesis of poly (β-amino ester)*: Poly(β-amino ester) (PAE) was synthesized via a Michael reaction between N, N- dimethylethylenediamine, and 1,4-butanediol diacrylate at the diacrylate: diamine ratio of 1.5:1, following the procedure explained in the literature.[69] Briefly, after the formation of 10% (v/v) diacrylate solution in DCM, the diamine monomer was added and reacted for 48 h at 50 °C. This solution was precipitated in diethyl ether and subsequently dried at ambient conditions for 5 days to eliminate residual ether. The synthesized PAE was stored at −20 °C for further studies.

Synthesis of Arg-N-PAE: The conjugation reaction of L-Arg to PAE (Arg-N-PAE) was performed was performed in the presence of EDC/NHS chemistry. Following the preparation of 10 wt.% PAE in double-distilled water (DDW) at ambient temperature, Arg was mixed with it to get a uniform solution. Subsequently, NHS and EDC-HCl were added to the mixture, while the weight ratio of EDC-HCl:NHS: polymer (Arg+PAE) was kept 1:1: 12 and mixed for 4 h at 4 °C. The Arg: PAE weight ratios were designed as 1:2, 1:3, and 1:5, respectively, and these resulting conjugates were named A2P, A3P, and A5P, respectively. The reaction solution was dialyzed using a 6–8 kDa cutoff dialysis membrane for 2 days against DDW with a daily change of the dialysate to remove unreacted reagents and by-products, followed by a freeze-drying process upon 48 h.

Synthesis of Arg-N-PAE/alginate particles: Aqueous solutions of sodium alginate and Arg-N-PAE with a concentration of 0.623 mg ml^{-1} were prepared in DDW and acetate buffers (pH = 5.6), respectively, overnight at room temperature. The polyelectrolyte complexes were prepared at room temperature at 800 rpm via dropwise adding alginate solution to the Arg-N-PAE solutions at a flow rate of 1 ml s^{-1}. Calcium chloride solution (18 mM) was added dropwise into the mixtures over 60 min to get stable particles. Arg-N-PAE: alginate weight ratios, were 2:1, 1:1, and 1:2. Depending on the Arg-N-PAE composition (A2P, A3P, and A5P), the particles were named A2PA, A3PA and A5PA, respectively. Moreover, Arg-free PAE was similarly used to develop PAE/alginate particles, called PA. Finally, the particles were kept with an additional stirring for 15 min to improve curing and then separated by centrifugation (10 000 g/20 min).

Preparation of the siRNA-Laden APA Polyplex: The siRNA-laden APA polyplexes at different APA: siRNA weight ratios (1:1, 10:1, 25:1, 100:1 to 200:1) were created by combining equal volumes of Flii siRNA solution with APA at a concentration of 0.623 mg ml^{-1} in sterile nuclease-free DEPC water. The solutions were mixed by pipetting and vertexing for 15 s, then allowed to incubate at room temperature for 10 min. Subsequently, an equal volume of 0.623 mg ml^{-1} alginate solution in sterile nuclease-free DEPC water was introduced, mixed, and incubated for an additional 10 min. As-prepared particles were centrifuged at 10 000 g for 10 min and kept at 4 °C for the following experiments. Control particles were freshly synthesized using LIP according to the manufacturer's instructions. siRNA and LIP were mixed with a constant weight ratio of 1:2.5 in Opti-MEM and preserved at room temperature for 15 min before use. The sample was named siRNA-LIP polyplex.

© 2024 The Author(s). Advanced Therapeutics published by Wiley-VCH GmbH

23663987, 2024, 12, Downloaded from https://advanced.onlinelibrary.wiley.com/doi/10.1002/adtp.202400329 by Universitaet Bayreuth, Wiley Online Library on [14/03/2025]. See the Terms and Conditions (https://onlinelibrary.wiley.com/terms-and-conditions) on Wiley Online Library for rules of use; OA articles are governed by the applicable Creative Commons License

Characterization of siRNA-Laden APA Polyplex: Fourier Transform Infrared (FTIR) spectra of precursors (PAE, Arg-N-PAE) and APA particles were recorded utilizing a germanium crystal on a Bruker Tensor 27. PAE and Arg-N-PAEs were also assessed by proton nuclear magnetic resonance (^{1}H-NMR) on an INOVA-400 spectrometer at 400 MHz. The solvent employed was deuterium oxide (D_2O, Cambridge Isotope Laboratories). The conjugation efficiency of Arg in the Arg-N-PAE copolymers was determined by the Sakaguchi reaction between Arg and ninhydrin, following a previously established protocol.[70] Briefly, 3 ml of the cold supernatant solution containing 0.04–0.07 mg of Arg was mixed with 1 ml of cold 10 wt.% sodium hydroxide solution and 1 ml of 0.02%(v/v) α-Naphthol solution in 0.1%(v/v) ethanol. After 3 min, 2 ml of hydrobromide solution (0.64 ml bromine in 100 ml of 5%(v/v) cold sodium hydroxide) was mixed with the above solution under vigorous stirring, and after 15 s, 1 ml of cold urea solution (5%(v/v)) was added. Finally, the absorbance of the solution was measured using UV–vis spectroscopy at 520 nm. Finally, the concentration of Arg was determined according to the standard curve of Arg (0–200 µM). The mean diameter, PDI, and z-potential of APA, siRNA-APA, and siRNA-LIP particles were determined at room temperature and a wavelength of 633 nm using DLS (Litesizer 500, Anton Paar). A volume of 100 µl of particles was mixed with 900 µl of DDW, and hydrodynamic size and z-potential analysis were recorded in triplicate. The z-potential was determined using Smoluchowski's theory, which relied on the measured electrophoretic mobility. The morphology of APA particles was investigated using a SEM (VCarl Zeiss Microscopy GmbH, and Apreo VS, Thermo Fisher Scientific, Germany). The complexes were diluted and carefully dripped on a glass plate which, after drying, was sputter-coated with 2 nm platinum.

Arginine Release Behavior: The in vitro Arg release from APA particles was studied over 24 h by the dialysis technique similar to previous studies.[71] For this purpose, 2 ml of APA particles as a suspension in PBS were dialyzed in a 15 ml dialysis tube of 6–8 kDa containing 10 ml PBS (pH 7.4) and were shaken in a falcon tube containing 30 ml of DDW as a release medium at 100 rpm at 37 °C. At predefined time intervals (1, 3, 12, 18, 24, 36, and 48 h), 300 µl of supernatant was collected from the tubes and replaced with PBS. The Sakaguchi reaction mentioned above quantitatively assessed the released Arg in the supernatant.

Flii siRNA Retardation Assay: Agarose gel electrophoresis was used to evaluate the role of APA on siRNA condensation and encapsulation. 15 µl of different APA: siRNA (w/w) ratios and plain siRNA were mixed with 10 µl of loading RNA and then loaded in 200 ml of 1.5 wt.% agarose gel in 1× Tris-Acetate-EDTA buffer (pH 8.6) containing SYBR Safe DNA Gel Stain (12 µl). Following the pipetting of 15 µl per line of samples and plain siRNA, electrophoresis was conducted at 80 V for 60 min (BluePower 500, SERVA). A 1 kb and 100 kb ladder were used as the references. Following the electrophoresis process, the resulting siRNA migration bands were visualized by UV light illumination using an Imaging System (Bio-Rad). Moreover, the gel electrophoresis assay was similarly performed on alginate-free polyplex (siRNA-Arg-N-PAE) to study the effect of alginate on the stability of polyplex. Furthermore, the concentration of loaded siRNA was indirectly assessed by measuring UV absorbance at 260 nm with a spectrophotometer (NanoDrop ND-1000 UV–Vis Spectrophotometer, Thermo Fisher Scientific). Subsequently, the dispersed particles underwent centrifugation to segregate the free siRNA from the siRNA-loaded pellets. Finally, the loading efficiency (LE%) was estimated using the following Equation (1):[71]

$$LE\ (\%) = \left[1 - \left(\frac{OD\ of\ sample\ in\ suspension}{OD\ of\ initial\ feeding\ amount\ of\ sample}\right)\right] \times 100 \quad (1)$$

Complex Stability Assay: Compared to LIP as the positive control, the complexes' stability was studied by the incubation of siRNA-APA and siRNA-LIP particles with heparin as a competitive binding agent, based on a competition assay. Briefly, an equal volume of polyplexes (15 µM) and heparin sodium salt were mixed using a vortex mixer. Different concentrations of heparin sodium salt solution (0.25, 1, 5, and 10 µg ml^{-1}) were added to polyplexes. Following 15 min incubation at room temperature, 15 µl of each sample underwent electrophoresis on an agarose gel stained with ethidium bromide for analysis, as mentioned above. Moreover, the free siRNA concentration was estimated using the spectrophotometer.

In Vitro Release of Flii siRNA: *In vitro,* siRNA release from siRNA-APA and siRNA-LIP polyplexes was examined using a spectrophotometer in PBS solution with pH 7.4 by the dialysis technique. In this regard, 0.2 mg ml^{-1} of samples were added into a dialysis tube (12–14 kDa) comprising 10 ml of PBS and shaken at 300 rpm at 37 °C. At specific time intervals (5 min, 4, 24, and 48 h), 500 µl of supernatant was collected from the tubes and then replenished with an equivalent volume of PBS. The release medium from unloaded APA particles was used as blank. Finally, the siRNA concentration in the supernatant was measured using a NanoDrop UV–Vis Spectrophotometer at 260 nm, and siRNA release (%) was estimated according to the following Equation (2):[71]

$$Released\ siRNA\ (\%) = \left(\frac{OD\ of\ siRNA\ in\ PBS}{OD\ of\ initial\ content\ of\ siRNA}\right) \times 100 \quad (2)$$

Cell Culture: The J774.1 mouse macrophage and BJ human skin fibroblast cell lines were used to determine cell/particle or polyplex interactions. J774.1 (ATCC TIB-67) cells were cultured in DMEM supplemented with 10%(v/v) FBS, 2%(v/v) HEPES, 2%(v/v) GlutaMax, 1%(v/v) sodium pyruvate, 1%(v/v) Pen/Strep. Moreover, BJ fibroblasts (ATCC CRL-2522) were cultured in EMEM supplemented with 10%(v/v) FBS, 1%(v/v) GlutaMax, and 0.1%(v/v) Gentamycin. The cells were incubated at 37 °C and 5% CO_2.

Cell Proliferation Evaluation: The cell proliferation in contact with APA particles and siRNA-APA polyplexes was evaluated using the Alamarblue assay in a 96-well plate with a density of 10000 J774.1 macrophage/well and BJ fibroblasts/well. To investigate the optimized concentration of particles, after reaching 30% confluency, the BJ cells were treated with various concentrations of particles (ranging from 0–200 mg ml^{-1}) in full medium and incubated for 24 h. Then, the cell proliferation was studied using the Alamarblue assay, according to the manufacturer's protocol. Briefly, the Alamarblue reagent was diluted 1:10 in full medium and added to the cells. After a 4 h incubation at 37 °C, medium fluorescence at 560/590 nm (excitation/emission) was determined using a plate reader (Mithras LB 940, Bertold). All the conditions were performed in triplicate. After optimization of APA particle concentration, the Alamarblue assay was performed similarly to investigate the proliferation of J774.1 cells in contact with particles and polyplexes. Moreover, cell viability was assessed in J774.1 and BJ cells using the live/dead assay with two fluorescent dyes, calcein AM and EthD-1, based on the manufacturer's protocol. Cells were seeded in 48-well plates (10000 J774.1 and BJ cells per well) and incubated for 24 h. Afterward, the cells were exposed to a 100 µl solution comprising calcein AM (2 µM) and EthD-1(4 µM) for 20 min. The cell viability was assessed following 24 and 48 h of treatment. Fluorescent imaging was performed utilizing a Leica DMI 3000B fluorescence microscope equipped with LAS X software (Leica).

Cell Migration Evolution Via Scratch Test: The migration of BJ fibroblast was assessed by monitoring cell expansion on the wound surface through a scratch assay. Fibroblasts were cultured into a 6-well plate at a density of 10^6 cells well^{-1} for 24 h until a monolayer formed. Next, the monolayer was scratched using a sterile 200 µl plastic pipette tip. Following three washes with PBS, 200 µl of particles in serum-free medium were added to each well, and the plate was further incubated for 48 h. Images of the cells were captured at 0, 4, 24, and 48 h using a Leica DM IL LED microscope and processed using LAS 4.8 software (Leica). Following the measuring of the wound area in each image using ImageJ software. The scratch closure rate was then quantified using Equation (3):

$$Scratch\ closure\ rate = \frac{\left[A_t - A_{t_0}\right]}{A_t} \times 100 \quad (3)$$

where A_{t0} and A_t represent the scratch area at the initial time point and the corresponding time point after incubation with particles. Moreover, Collagen type I (Col I) deposition after the scratch test was assessed through a quantitative polymerase chain reaction (qPCR) assay. RNA extraction was performed using the innuMIX qPCR DSGreen Standard kit following the

© 2024 The Author(s). Advanced Therapeutics published by Wiley-VCH GmbH

23663987, 2024, 12, Downloaded from https://advanced.onlinelibrary.wiley.com/doi/10.1002/adtp.202400329 by Universitaet Bayreuth, Wiley Online Library on [14/03/2025]. See the Terms and Conditions (https://onlinelibrary.wiley.com/terms-and-conditions) on Wiley Online Library for rules of use; OA articles are governed by the applicable Creative Commons License

manufacturer's protocol. Reverse transcription was performed to acquire the complementary DNA (cDNA) using RevertAid First Strand cDNA Synthesis Kit, according to the manufacturer's instructions. Following PCR reaction in a qTOWER 2.0 system (Analytik Jena), the data were analyzed using qPCRsoft (Analytik Jena AG) software. The primer sequences of the target genes re provided in Table S1 (Supporting Information). DNA amplification was done under the following conditions: 2 min at 95± 3 °C, 40 cycles of 10 s at 95 °C and 30 s at 60 °C, and 1 cycle of 5 sec/step at 65–95 °C. The amplification efficiency of the Col I gene was normalized to the housekeeping gene (Cyclophilin A, CypA).

NO Production: J774.1 macrophages (4×10^5 cells mL^{-1}) were seeded on a 6-well plate to investigate the role of APA-based particles in modulating NO production. After reaching 70% confluency, the medium was substituted with a serum-free medium supplemented with LPS (100 ng ml^{-1}) to polarize them into M1 macrophages, according to previous studies.[55] After 24 h, cells were washed with PBS, treated with 100 µg ml^{-1} of APA-based particles, and incubated for 24 h at 37 °C. Macrophages incubated in DMEM containing 10 v/v% FBS without treatments were applied as controls. The NO production was determined using Griess reagent according to the manufacturer's protocol (Sigma). The absorbance of the solutions was recorded at 540 nm within 30 min and, the NO production was quantified by the nitrite concentration in the supernatant, determined from a nitrite standard reference curve.

Intracellular Uptake Analysis and Mechanism: For intercellular uptake of APA particles, alginate was labeled with Rhodamine. In this regard, after preparation of EDC-HCl (0.1 g) and NHS (0.05 g) solution in 0.1 M MES buffer (1 ml) at pH = 6, 1 mg of 5(6)-carboxy-x-Rhodamine was added. Consequently, 5 mg of alginate was added to the solution and allowed to react overnight. The labeled alginate was dialyzed against DDW for 2 days and finally was lyophilized. The labeled alginate was used in the formation of APA particles instead of the unlabeled alginate. The particle uptake was studied in both J774.1 macrophages and BJ fibroblasts, seeded in a 6-well plate at densities of 4×10^5 and 1×10^6 cells $well^{-1}$, respectively. After 24 h, the medium was substituted with 2 ml of APA particles or siRNA-based polyplexes and further incubated for 6 and 24 h. The cells were harvested for flow cytometry assessment by Cytomics FC500 (Beckman-Coulter). Untreated cells served as the negative control group. Moreover, to investigate the uptake of siRNA-APA polyplexes, siRNA-LIP, and plain siRNA were used as positive controls. The efficiency of cellular uptake was reflected by the intensity of internalized Rhodamine-labeled particles and Flii Rh-siRNA. Moreover, for the confocal microscopy analyses, cells were seeded onto µ-slides (8-well, ibidi GmbH) at a density of 2×10^4 cells cm^2 and treated with Rhodamine-labeled particles for 24 h. Subsequently, the cells were fixed with PFA (4%(v/v)), rinsed with PBS, and permeabilized with Triton 100x (0.1%(v/v), 5 min). Following PBS washing, cells were stained with Alexa Fluor 488 Phalloidin solution (1:40 dilution in PBS, 30 min) and DAPI solution (1:1000 in PBS, 5 min). Fluorescence microscopy and a DMI 8 confocal laser scanning microscope equipped with lasers were used for imaging, and LAS X software (Leica) was employed for data analysis. Three individual images were captured for each sample group (n = 3).

To evaluate the cellular uptake mechanisms of APA particles, endocytic inhibitors were used in the case of macrophages in 6-well plates, similar to the procedure described above. The experiment was divided into 3 groups, namely, positive control, and 2 treatment groups. For the treatment groups, the J774.1 macrophages were treated with 100 µM DC (the clathrin-mediated endocytic inhibitor) or 100 µM DMA (the micropinocytosis inhibitor) in the serum-free medium for 6 h. Control groups were APA-treated cells incubated in a serum-free medium for 6 h. Following the incubation period, the cells underwent two washes with PBS, after which flow cytometry was employed to assess the cellular uptake of APA particles.

The Transfection Efficiency: The transfection effectiveness of polyplexes was examined in BJ fibroblast cells. Cells were cultured in a 6-well plate at an initial seeding density of 4×10^5 cells $well^{-1}$, reaching 80%–90% confluency before conducting the transfection experiments. Subsequently, cells were transfected with siRNA-APA in the Opti-MEM medium. siRNA-LIP polyplex, APA particles, and plain siRNA were used as positive controls. Moreover, untreated cells were used as the negative control. Following 6 h incubation of polyplexes (250 µl) at 37 °C in a 5% CO_2, the remaining complexes were replaced with 500 µL of complete DMEM medium to incubate for 24 h for knockdown gene assessment. To evaluate Flii siRNA-induced knockdown and its effects on wound healing, the qPCR assay was performed with Flii and Col I gene-specific primers (Table S1, Supporting Information). The quantification was first normalized to CypA as the housekeeping gene to obtain values for fold change. The protocol was performed, as mentioned in section 2.9.2.

Furthermore, Flii siRNA-induced knockdown was further studied using the immunostaining for Flii-specific protein after 1 and 2 days of culture, following the manufacturer's instructions (Invitrogen). In this regard, after the fixation and permeabilization of cells using PFA solution (3.5%(v/v), 20 min) and Triton 100× (0.1%(v/v), 5 min), respectively, the cells were blocked in BSA solution (10 wt.%, 30 min). Then, a 1:400 (0.25 µg ml^{-1}) dilution of primary antibody (Flii Polyclonal Antibody) in FBS (10%(v/v)) was added to the samples, and they were incubated at 4 °C overnight. Following three washes with PBS, a 1:200 dilution of Alexa Fluor 488 goat anti-rabbit IgG secondary antibody in FBS (10%(v/v)) was applied to the samples. Following incubation in the dark for 40 min, the cells' nuclei were stained using a 1:1000 (v/v) dilution of DAPI in PBS (5 min). Subsequently, the samples were observed using a fluorescence microscope, and the images were processed using Image J software.

Immunomodulatory Properties: As an in vitro cell culture model, J774.1 macrophages were applied to determine the anti-inflammatory properties of APA particles and polyplexes by determining the level of anti-inflammation of TGF-β and Arg-1 (M1 markers) and their pro-inflammatory effect by measuring the level ofTNF-α, IL6 as M2 markers. In this regard, the cells were seeded in 6-well plates at a density of 10^6 cells/ and induced to an M1 phenotype by incubating overnight with LPS (100 ng ml^{-1}). Subsequently, the M1 macrophages were transfected with 50 µg ml^{-1} particles in Opti-MEM I medium for 24 h. Following the harvesting of the cells, the gene expression levels were quantified using a qPCR assay. GAPDH was applied as the housekeeping gene. The primer sequence of the target genes is provided in Table S1 (Supporting Information).

Statistical Analysis: The findings were reported as mean ± standard deviation. Statistical analysis to compare between groups was conducted using One-way ANOVA and GraphPad software (La Jolla, version 8). A $P < 0.05$ was considered statistically significant.

Supporting Information

Supporting Information is available from the Wiley Online Library or from the author.

Acknowledgements

This work was supported by Deutsche Forschungsgemeinschaft DFG (SA 3575/2–1) Project number 497840077. Furthermore, M.K. acknowledges the Alexander von Humboldt (AvH) Foundation for providing the experienced researcher fellowship.

Open access funding enabled and organized by Projekt DEAL.

Conflict of Interest

The authors declare no conflict of interest.

Data Availability Statement

The data that support the findings of this study are available from the corresponding author upon reasonable request.

Keywords

arginine, chronic wounds, Flii siRNA, immunomodulatory properties, poly(β-amino ester)

© 2024 The Author(s). Advanced Therapeutics published by Wiley-VCH GmbH

23663987, 2024, 12, Downloaded from https://advanced.onlinelibrary.wiley.com/doi/10.1002/adtp.202400329 by Universitaet Bayreuth, Wiley Online Library on [14/03/2025]. See the Terms and Conditions (https://onlinelibrary.wiley.com/terms-and-conditions) on Wiley Online Library for rules of use; OA articles are governed by the applicable Creative Commons License

Received: July 25, 2024
Revised: August 30, 2024
Published online: October 23, 2024

[1] P. Krzyszczyk, R. Schloss, A. Palmer, F. Berthiaume, *Front. Physiol.* **2018**, *9*, 419.
[2] D. M. Mosser, J. P. Edwards, *Nat. Rev. Immunol.* **2008**, *8*, 958.
[3] J. Mao, L. Chen, Z. Cai, S. Qian, Z. Liu, B. Zhao, Y. Zhang, X. Sun, W. Cui, *Adv. Funct. Mater.* **2022**, *32*, 2111003.
[4] a) A. Gulzar, J. Xu, C. Wang, F. He, D. Yang, S. Gai, P. Yang, J. Lin, D. Jin, B. Xing, *Nano Today* **2019**, *26*, 16; b) M. Kharaziha, A. Baidya, N. Annabi, *Adv. Mater.* **2021**, *33*, 2100176; c) S. Khodakarimi, A. Zarebkohan, H. Kahroba, M. Omrani, T. Sepasi, G. Mohaddes, H. Beyrampour-Basmenj, A. Ebrahimi, A. Ebrahimi-Kalan, *Life Sci.* **2021**, *287*, 119726.
[5] C. Papara, D. Zillikens, C. D. Sadik, A. Baican, *Autoimmun Rev.* **2021**, *20*, 102852.
[6] A. J. Cowin, N. Lei, L. Franken, N. Ruzehaji, C. Offenhäuser, Z. Kopecki, R. Z. Murray, *Commun. Integr. Biol.* **2012**, *5*, 546.
[7] N. van Beek, E. Schmidt, *Harper's Textbook Pediat. Dermatol.* **2019**, 68.
[8] M. Zeng, Q. Xu, D. Zhou, A. Sigen, F. Alshehri, I. Lara-Sáez, Y. Zheng, M. Li, W. Wang, *Adv. Drug Delivery Rev.* **2021**, *176*, 113842.
[9] J. Gan, C. Liu, H. Li, S. Wang, Z. Wang, Z. Kang, Z. Huang, J. Zhang, C. Wang, D. Lv, L. Dong, *Biomaterials* **2019**, *219*, 119340.
[10] Z. Siprashvili, N. T. Nguyen, E. S. Gorell, K. Loutit, P. Khuu, L. K. Furukawa, H. P. Lorenz, T. H. Leung, D. R. Keene, K. E. Rieger, P. Khavari, *JAMA, J. Am. Med. Assoc.* **2016**, *316*, 1808.
[11] S. Turczynski, M. Titeux, L. Tonasso, A. Décha, A. Ishida-Yamamoto, A. Hovnanian, *J. Invest. Dermatol.* **2016**, *136*, 2387.
[12] P. Sharma, A. Kumar, T. Agarwal, A. D. Dey, F. D. Moghaddam, I. Rahimmanesh, M. Ghovvati, S. Yousefiasl, A. Borzacchiello, A. Mohammadi, V. R. Yella, *Int. J. Biol. Macromol.* **2022**, *220*, 920.
[13] B. Lan, L. Zhang, L. Yang, J. Wu, N. Li, C. Pan, X. Wang, L. Zeng, L. Yan, C. Yang, M. Ren, *J. Nanobiotechnol.* **2021**, *19*, 130.
[14] a) Y. Weng, H. Xiao, J. Zhang, X. J. Liang, Y. Huang, *Biotechnol. Adv.* **2019**, *37*, 801; b) H. Yuan-Yu, *Progress Biochem. Biophys.* **2019**, *46*, 313; c) M. Zheng, Y. Liu, Y. Wang, D. Zhang, Y. Zou, W. Ruan, J. Yin, W. Tao, J. B. Park, B. Shi, *Adv. Mater.* **2019**, *31*, 1903277.
[15] a) C. Yu, L. Li, P. Hu, Y. Yang, W. Wei, X. Deng, L. Wang, F. R. Tay, J. Ma, **2021**, *8*, 2100540; b) R. A. Cordeiro, A. Serra, J. F. Coelho, H. Faneca, *J. Controlled Release* **2019**, *310*, 155.
[16] H. Rahimi, M. Salehiabar, J. Charmi, M. Barsbay, M. Ghaffarlou, M. R. Razlighi, S. Davaran, R. Khalilov, M. Sugiyama, H. Nosrati, S. Kaboli, *Nano Today* **2020**, *34*, 100895.
[17] G. Sahay, W. Querbes, C. Alabi, A. Eltoukhy, S. Sarkar, C. Zurenko, E. Karagiannis, K. Love, D. Chen, R. Zoncu, Y. Buganim, *Nat. Biotechnol.* **2013**, *31*, 653.
[18] M. Kharaziha, T. Scheibel, S. Salehi, *Prog. Polym. Sci.* **2024**, 101792.
[19] Y. Liang, Y. Wang, L. Wang, Z. Liang, D. Li, X. Xu, Y. Chen, X. Yang, H. Zhang, H. Niu, *Bioactive Mater.* **2021**, *6*, 433.
[20] P. Zhupanyn, A. Ewe, T. Büch, A. Malek, P. Rademacher, C. Müller, A. Reinert, Y. Jaimes, A. Aigner, *J. Controlled Release* **2020**, *319*, 63.
[21] Y. Rui, M. Varanasi, S. Mendes, H. M. Yamagata, D. R. Wilson, J. J. Green, *Mol. Ther.-Nucleic Acids* **2020**, *20*, 661.
[22] P. Wu, H. Chen, R. Jin, T. Weng, J. K. Ho, C. You, L. Zhang, X. Wang, C. Han, *J. Translat. Med.* **2018**, *16*, 29.
[23] E. Shaabani, M. Sharifiaghdam, H. De Keersmaecker, R. De Rycke, S. De Smedt, R. Faridi-Majidi, K. Braeckmans, J. C. Fraire, *Int. J. Mol. Sci.* **2021**, *22*, 831.
[24] A. Vedadghavami, C. Zhang, A. G. Bajpayee, *Nano Today* **2020**, *34*, 100898.
[25] a) L. N. Kasiewicz, K. A. Whitehead, *Bioeng. Transl. Med.* **2019**, *4*, 75; b) A. Ahmad, J. M. Khan, S. Haque, *Biochimie* **2019**, *160*, 61.
[26] N. Distasio, F. Dierick, T. Ebrahimian, M. Tabrizian, S. Lehoux, *Acta Biomater.* **2022**, *143*, 356.
[27] R. Núñez-Toldrà, P. Dosta, S. Montori, V. Ramos, M. Atari, S. Borrós, *Acta Biomater.* **2017**, *53*, 152.
[28] P. Dosta, V. Ramos, S. Borrós, *Mol. Syst. Des. Eng.* **2018**, *3*, 677.
[29] Z. Ling, J. Deng, Z. Zhang, H. Sui, W. Shi, B. Yuan, H. Lin, X. Yang, J. Cao, X. Zhu, X. Zhang, *Appl. Mater. Today* **2021**, *24*, 101116.
[30] a) D. Q. Wu, J. Zhu, H. Han, J. Z. Zhang, F. F. Wu, X. H. Qin, J. Y. Yu, *Acta Biomater.* **2018**, *65*, 305; b) Y. Zhou, G. Liu, H. Huang, J. Wu, *J. Mater. Chem. B* **2021**, *9*, 6738.
[31] J. B. Rothbard, S. Garlington, Q. Lin, T. Kirschberg, E. Kreider, P. L. McGrane, P. A. Wender, P. A. Khavari, *Nat. Med.* **2000**, *6*, 1253.
[32] Y. Zhou, S. Han, Z. Liang, M. Zhao, G. Liu, J. Wu, *J. Mater. Chem. B* **2020**, *8*, 5564.
[33] N. Segovia, M. Pont, N. Oliva, V. Ramos, S. Borrós, N. Artzi, *Adv. Healthcare Mater.* **2015**, *4*, 271.
[34] P. Dosta, N. Segovia, A. Cascante, V. Ramos, S. Borrós, *Acta Biomater.* **2015**, *20*, 82.
[35] N. Segovia, P. Dosta, A. Cascante, V. Ramos, S. Borrós, *Acta Biomater.* **2014**, *10*, 2147.
[36] W. Li, J. Sun, X. Zhang, L. Jia, M. Qiao, X. Zhao, H. Hu, D. Chen, Y. Wang, *Pharmaceutics* **2020**, *12*, 111.
[37] a) J. Zhu, L. Liao, L. Zhu, P. Zhang, K. Guo, J. Kong, C. Ji, B. Liu, *Talanta* **2013**, *107*, 408; b) L. Li, W. S. Xi, Q. Su, Y. Li, G. H. Yan, Y. Liu, H. Wang, A. Cao, *Small* **2019**, *15*, 1901687.
[38] J. Stetefeld, S. A. McKenna, T. R. Patel, *Biophys. Rev.* **2016**, *8*, 409.
[39] K. Obst, G. Yealland, B. Balzus, E. Miceli, M. Dimde, C. Weise, M. Eravci, R. Bodmeier, R. Haag, M. Calderón, N. Charbaji, *Biomacromolecules* **2017**, *18*, 1762.
[40] Z. Mohammadpour, M. Kharaziha, A. Zarrabi, M. Fathi, *Carbon* **2017**, *111*, 752.
[41] S. A. Malik, A. A. Dar, J. A. Banday, *Colloids Surf. A* **2023**, *663*, 131046.
[42] D. M. Lynn, R. Langer, *J. Am. Chem. Soc.* **2000**, *122*, 10761.
[43] a) M. He, A. Potuck, Y. Zhang, C. C. Chu, *Acta Biomater.* **2014**, *10*, 2482; b) M. Yin, S. Wan, X. Ren, C. C. Chu, *ACS Appl. Mater. Interfaces* **2021**, *13*, 14688.
[44] M. He, C. C. Chu, *Polymer* **2023**, *54*, 4112.
[45] X. Ma, Y. Cheng, H. Jian, Y. Feng, Y. Chang, R. Zheng, X. Wu, L. Wang, X. Li, H. Zhang, *Adv. Healthcare Mater.* **2019**, *8*, 1900256.
[46] L. Zou, Q. Peng, P. Wang, B. Zhou, *The Journal of membrane biology* **2017**, *250*, 115.
[47] B. J. Calnan, B. Tidor, S. Biancalana, D. Hudson, A. D. Frankel, *Science* **1991**, *252*, 1167.
[48] a) M. C. Hamoudi, E. Henry, N. Zerrouk, D. Scherman, P. Arnaud, E. Deprez, V. Escriou, *J. Drug Del. Sci. Technol.* **2015**, *26*, 1. b) D. C. Arruda, I. J. Gonzalez, S. Finet, L. Córdova, V. Trichet, G. F. Andrade, C. Hoffmann, P. Bigey, W. A. de Almeida Macedo, A. D. S. Cunha Jr., A. M. de Souza, *J. Colloid Interface Sci.* **2019**, *540*, 342; c) T. Li, G. D. Wang, Y. Z. Tan, H. J. Wang, *Int. J. Biol. Sci.* **2014**, *10*, 160.
[49] J. B. Rothbard, T. C. Jessop, R. S. Lewis, B. A. Murray, P. A. Wender, *J. Am. Chem. Soc.* **2004**, *126*, 9506.
[50] L. A. Fliervoet, H. Zhang, E. van Groesen, K. Fortuin, N. J. Duin, K. Remaut, R. M. Schiffelers, W. E. Hennink, T. Vermonden, *Nanoscale* **2020**, *12*, 10347.

© 2024 The Author(s). Advanced Therapeutics published by Wiley-VCH GmbH

23663987, 2024, 12, Downloaded from https://advanced.onlinelibrary.wiley.com/doi/10.1002/adtp.202400329 by Universitaet Bayreuth, Wiley Online Library on [14/03/2025]. See the Terms and Conditions (https://onlinelibrary.wiley.com/terms-and-conditions) on Wiley Online Library for rules of use; OA articles are governed by the applicable Creative Commons License

[51] N. Chen, Y. He, M. Zang, Y. Zhang, H. Lu, Q. Zhao, S. Wang, Y. Gao, *Biomaterials* **2022**, *286*, 121567.
[52] S. Ray, X. Ju, H. Sun, C. C. Finnerty, D. N. Herndon, A. R. Brasier, *J. Invest. Dermatol.* **2013**, *133*, 1212.
[53] C. T. Turner, M. Hasanzadeh Kafshgari, E. Melville, B. Delalat, F. Harding, E. Mäkilä, J. J. Salonen, A. J. Cowin, N. H. Voelcker, *ACS Biomater. Sci. Eng.* **2016**, *2*, 2339.
[54] Z. Ling, Z. Chen, J. Deng, Y. Wang, B. Yuan, X. Yang, H. Lin, J. Cao, X. Zhu, X. Zhang, *Chem. Eng. J.* **2021**, *420*, 130302.
[55] T. Kawakami, K. Kawamura, K. Fujimori, A. Koike, F. Amano, *Biochem. Biophys. Reports* **2016**, *5*, 328.
[56] A. Koike, I. Minamiguchi, K. Fujimori, F. Amano, *Biol. Pharmaceut. Bull.* **2015**, *38*, 7.
[57] M. Rizk, M. B. Witte, A. Barbul, *World J. Surg.* **2004**, *28*, 301.
[58] J. E. Park, M. J. Abrams, P. A. Efron, A. Barbul, *J. Surg. Res.* **2013**, *183*, 487.
[59] O. Lunov, T. Syrovets, C. Loos, J. Beil, M. Delacher, K. Tron, G. U. Nienhaus, A. Musyanovych, V. Mailander, K. Landfester, T. Simmet, *ACS Nano* **2011**, *5*, 1657.
[60] C. L. Roy, J. L. Wrana, *Nat. Rev. Mol. Cell Biol.* **2005**, *6*, 112.
[61] Y. Rui, D. R. Wilson, J. Choi, M. Varanasi, K. Sanders, J. Karlsson, M. Lim, J. J. Green, *Sci. Adv.* **2019**, *5*, eaay3255.
[62] B. Saleh, H. K. Dhaliwal, R. Portillo-Lara, E. Shirzaei Sani, R. Abdi, M. M. Amiji, N. Annabi, *Small* **2019**, *15*, 1902232.
[63] B. Bueno-Silva, P. L. Rosalen, S. M. Alencar, M. P. Mayer, *Int. Immunopharmacol.* **2020**, *82*, 106329.
[64] S. Wang, R. Liu, Q. Yu, L. Dong, Y. Bi, G. Liu, *Cancer Lett.* **2019**, *452*, 14.
[65] K. Eghbalzadeh, L. Georgi, T. Louis, H. Zhao, U. Keser, C. Weber, M. Mollenhauer, A. Conforti, T. Wahlers, A. Paunel-Görgülü, *Front. Immunol.* **2019**, *10*, 2313.
[66] M. Nolte, C. Margadant, *Trends Cell Biol.* **2020**, *30*, 49.
[67] R. R. Arvizo, O. R. Miranda, M. A. Thompson, C. M. Pabelick, R. Bhattacharya, J. D. Robertson, V. M. Rotello, Y. S. Prakash, P. Mukherjee, *Nano Lett.* **2010**, *10*, 2543.
[68] a) M. J. Mitchell, M. M. Billingsley, R. M. Haley, M. E. Wechsler, N. A. Peppas, R. Langer, *Nat. Rev. Drug Discovery* **2021**, *20*, 101; b) L. Wu, W. Zhou, L. Lin, A. Chen, J. Feng, X. Qu, H. Zhang, J. Yue, *Bioactive Mater.* **2022**, *7*, 101.
[69] P. Heydari, J. Varshosaz, M. Kharaziha, S. H. Javanmard, *J. Mater. Sci.: Mater. Med.* **2023**, *34*, 16.
[70] E. Jorpes, S. Thorén, *Biochem. J.* **1932**, *26*, 1504.
[71] N. M. Zolbanin, R. Jafari, J. Majidi, F. Atyabi, M. Yousefi, F. Jadidi-Niaragh, L. Aghebati-Maleki, D. Shanehbandi, M. S. S. Zangbar, A. M. Nayebi, *Adv. Pharm. Bull.* **2018**, *8*, 383.

© 2024 The Author(s). Advanced Therapeutics published by Wiley-VCH GmbH

23663987, 2024, 12, Downloaded from https://advanced.onlinelibrary.wiley.com/doi/10.1002/adtp.202400329 by Universitaet Bayreuth, Wiley Online Library on [14/03/2025]. See the Terms and Conditions (https://onlinelibrary.wiley.com/terms-and-conditions) on Wiley Online Library for rules of use; OA articles are governed by the applicable Creative Commons License